American Mineralogist, Volume 92, pages 328–343, 2007

Elastic anomalies accompanying phase transitions in $(Ca,Sr)TiO_3$ perovskites: Part II. Calibration for the effects of composition and pressure

MICHAEL A. CARPENTER*

Department of Earth Sciences, University of Cambridge, Downing Street, Cambridge CB2 3EQ, U.K.

ABSTRACT

A Landau free energy expansion has been developed in a first attempt to describe the $Pm\bar{3}m \leftrightarrow I4/mcm$ octahedral tilting transition in perovskite across a complete binary solid solution, $CaTiO_3$-$SrTiO_3$ (CST). Only two parameters, the critical temperature and the coefficient, λ_4, for coupling between the order parameter and the tetragonal strain are given a composition-dependence. The best match between observed and calculated variations of the tetragonal strain as a function of temperature in $CaTiO_3$ (CST0) and as a function of composition at room temperature is found for a model of the solid solution in which the transition is close to tricritical for the composition range CST0 to ~CST90. The change in transition character from second order (246 potential) to tricritical is accounted for by an increase in $|\lambda_4|$ between $SrTiO_3$ (CST100) and ~CST90. The Landau potential is used to calculate the variations of single-crystal and bulk elastic constants through the $Pm\bar{3}m \leftrightarrow I4/mcm$ transition as functions of both pressure and composition. This model for the CST solid solution permits the classical softening effects of strain/order parameter coupling to be separated quantitatively from the much larger superelastic softening observed for twinned crystals of tetragonal $SrTiO_3$ and CST. Data from the literature for relative changes of elastic properties measured at low frequencies have been rescaled to absolute values for comparison with calculated values of Young's modulus. These appear to show that, below the temperature for domain wall pinning, some 5–10% of softening of the isotropic Young's modulus could still be due to the effects of twin wall movements.

Keywords: Landau theory, elastic constants, phase transitions, $CaTiO_3$-$SrTiO_3$ solid solution

INTRODUCTION

The $CaTiO_3$-$SrTiO_3$ (CST) solid solution contains perovskites with $Pm\bar{3}m$, $I4/mcm$, and $Pnma$ symmetry, which appear to be closely analogous to the possible structural states of $(Mg,Fe)SiO_3$ and $CaSiO_3$ perovskites. Phase transitions in this system are also easily accessible to in-situ experimental investigation, making them particularly suitable for examining elastic anomalies that accompany changes in structure due to variations in temperature, composition or pressure. It is not necessarily the case that phase transitions occur between the equivalent structural states of silicate perovskites at pressure/temperature conditions within the Earth's mantle, but studies of elastic anomalies accompanying displacive phase transitions in CST perovskites should provide constraints on the style and magnitude of elastic anomalies that accompany transitions in many perovskite solid solutions as well as in other oxide or silicate phases with ferroelastic instabilities. The present paper is the second in a series of three on this topic. In the first paper (Carpenter 2007), a fully parameterized Landau expansion for the $Pm\bar{3}m \leftrightarrow I4/mcm$ transition in $SrTiO_3$ was tested against diverse experimental data from the literature. The same Landau expansion is used here in a first attempt to produce a quantitative model for the same transition across the entire CST solid solution. In the third paper (Carpenter et al. 2007), new experimental data for bulk and shear moduli obtained as a function of composition and as a function of pressure are used to test the model.

Changes in elastic properties accompanying structural phase transitions can generally be attributed to two basic mechanisms. An intrinsic softening occurs as a consequence of coupling between spontaneous strains, e, and the driving order parameter, Q. In essence, application of stress causes an elastic deformation, following Hooke's law, plus an additional relaxation as the order parameter adjusts to the new strain state. The effect is well understood and conforms to standard solutions of Landau free energy expansions (Slonczewski and Thomas 1970, and many subsequent studies). For a relatively recent review of the overall approach to analyzing this elastic behavior, see Carpenter and Salje (1998). In principle, it should be possible to devise a single Landau free energy expansion to describe the strain and elastic behavior of a system in which the symmetry change can be driven by changes in temperature, pressure, and composition. The second important softening mechanism involves movement of twin walls that arise at ferroelastic phase transitions. The amount of softening can be substantially greater than the intrinsic softening due to strain/order parameter coupling, leading to the concept of "superelastic" behavior (Schranz et al. 1999; Kityk et al. 2000a, 2000b; Binder and Knorr 2001; Lemanov et al. 2002; Harrison and Redfern 2002; Harrison et al. 2003, 2004a, 2004b, 2004c). Externally applied stresses cause the twin walls to move, resulting in a strain that can be much greater than the strain due to deforming regions of the crystal between the twin

* E-mail: mc43@esc.cam.ac.uk

walls. Movement of twin walls involves some dissipation so that the elastic softening is characterized also by increases in attenuation, and different theory is required to describe the temperature and frequency dependence (Fossheim and Berre 1972; Schranz et al. 1999; Kityk et al. 2000a, 2000b; Binder and Knorr 2001; Lemanov et al. 2002; Harrison and Redfern 2002; Harrison et al. 2003, 2004a, 2004b).

End-members of the CST system undergo phase transitions with falling temperature in the sequence $Pm\bar{3}m \leftrightarrow I4/mcm \leftrightarrow Pnma$ for $CaTiO_3$ (Redfern 1996; Kennedy et al. 1999; Carpenter et al. 2001) and $Pm\bar{3}m \leftrightarrow I4/mcm$ for $SrTiO_3$ (see bibliography in Carpenter 2007). The same transitions have been traced across the solid solution by in-situ methods at high temperatures (Qin et al. 2000; Harrison et al. 2003). For Sr-rich compositions and temperatures below room temperature, the sequence of transitions is rather more controversial, involving possible structures with space groups *Pbcm*, *Cmcm*, and *Imma* (Ball et al. 1998; Ranjan et al. 2000, 2001; Ranjan and Pandey 2001a, 2001b; Mishra et al. 2002, 2005, 2006a, 2006b; Ouillon et al. 2002; Ranson et al. 2005). *Cmcm* has been ruled out for the stable structure at intermediate compositions and room temperature, however (Howard et al. 2001; Ranjan et al. 2001), and the suggestion of *Imma* over a wide temperature interval in the composition range CST64–CST95 contradicts single-crystal X-ray diffraction data that favor *I*4/*mcm* for CST65 at room temperature (Yamanaka et al. 2002). Woodward et al. (2006) have proposed, on the basis of electron diffraction evidence, that the true symmetry in this composition range at room temperature may in fact be monoclinic. Nevertheless, the unit-cell dimensions remain metrically tetragonal within the standard experimental uncertainties from powder X-ray diffraction experiments (Ball et al. 1998). Recent synchrotron X-ray diffraction data for a sample with composition $(Ca_{0.30}Sr_{0.70})TiO_3$ are also consistent with space group *I*4/*mcm* (Howard et al. 2005). For the present analysis, the high temperature transition is assumed to involve the symmetry change $Pm\bar{3}m \leftrightarrow I4/mcm$. At the most Sr-rich compositions, a further transition is believed to occur below ~35 K (Bednorz and Müller 1984). The structure of the low temperature form is believed to have point group *mm*2 (Bianchi et al. 1994; Kleemann et al. 1997) but is not considered further here.

At high pressures, $CaTiO_3$ remains orthorhombic (Gillet et al. 1993; Ross and Angel 1999), but $SrTiO_3$ transforms to the *I*4/*mcm* structure (Ishidate et al. 1988; Bonello et al. 1989a, 1989b; Fischer et al. 1989; Ishidate and Isonuma 1992; Grzechnik et al. 1997). There appears to be only one study of the high-pressure behavior of CST samples with intermediate compositions, that of Yamanaka et al. (2002), who reported that $Ca_{0.35}Sr_{0.65}TiO_3$ (CST65) is tetragonal at ambient conditions and orthorhombic at 3.5 GPa.

This paper focuses on the $Pm\bar{3}m \leftrightarrow I4/mcm$ transition and is divided into five main sections. The 246 Landau expansion calibrated for $SrTiO_3$ in Carpenter (2007) is first extended to include the effects of composition and hydrostatic pressure. Phase diagrams for CST at high temperatures (ambient pressure) and high pressures (ambient temperature) are then presented. The following section sets out the calibration and testing of composition-dependent parameters, which are used to predict single-crystal and bulk elastic constant variations. Real CST samples display additional softening effects due to domain wall mobility, so, in the final section, experimental data from the literature are reanalyzed on the basis that the contributions of classical strain/order parameter coupling can now be separated quantitatively.

LANDAU THEORY

The starting point for an analysis of the effects of composition and pressure on phase transitions in (Ca,Sr)TiO_3 perovskites is the assumption that coefficients in the Landau expansion for $SrTiO_3$ remain constant across the solid solution. In the first instance, the only variable parameters are considered to be the transition temperatures. When considering the effect of composition on the $Pm\bar{3}m \leftrightarrow I4/mcm$ transition, Equation 5 of Carpenter (2007)becomes

$$\begin{aligned} G = {} & \frac{1}{2}a_2\Theta_{s2}\left(\coth\left(\frac{\Theta_{s2}}{T}\right)-\coth\left(\frac{\Theta_{s2}}{T_{c2x}}\right)\right)\left(q_4^2+q_5^2+q_6^2\right)+\frac{1}{4}b_2\left(q_4^2+q_5^2+q_6^2\right)^2 \\ & +\frac{1}{4}b_2'\left(q_4^4+q_5^4+q_6^4\right)+\frac{1}{6}c_2\left(q_4^2+q_5^2+q_6^2\right)^3+\frac{1}{6}c_2'\left(q_4q_5q_6\right)^2 \\ & +\frac{1}{6}c_2''\left(q_4^2+q_5^2+q_6^2\right)\left(q_4^4+q_5^4+q_6^4\right)+\lambda_2e_a\left(q_4^2+q_5^2+q_6^2\right) \\ & +\lambda_4\left[\sqrt{3}e_o\left(q_5^2-q_6^2\right)+e_t\left(2q_4^2-q_5^2-q_6^2\right)\right]+\lambda_5\left(e_4q_4q_6+e_5q_4q_5+e_6q_5q_6\right) \\ & +\frac{1}{4}\left(C_{11}^o-C_{12}^o\right)\left(e_o^2+e_t^2\right)+\frac{1}{6}\left(C_{11}^o+2C_{12}^o\right)e_a^2+\frac{1}{2}C_{44}^o\left(e_4^2+e_5^2+e_6^2\right), \end{aligned} \quad (1)$$

where T_{c2x} is the composition-dependent critical temperature. The renormalized form of this, with $q_4 \neq 0$, $q_5 = q_6 = 0$ (for the *I*4/*mcm* structure), is

$$G = \frac{1}{2}a_2\Theta_{s2}\left(\coth\left(\frac{\Theta_{s2}}{T}\right)-\coth\left(\frac{\Theta_{s2}}{T_{c2x}}\right)\right)q_4^2+\frac{1}{4}\left(b_2^*+b_2'^*\right)q_4^4+\frac{1}{6}\left(c_2+c_2''\right)q_4^6. \quad (2)$$

The equilibrium variation of q_4 is given by

$$q_4^2 = \frac{-\left(b_2^*+b_2'^*\right)+\sqrt{\left(b_2^*+b_2'^*\right)^2+4a_2\left(c_2+c_2''\right)\Theta_{s2}\left(\coth\left(\frac{\Theta_{s2}}{T_{c2x}}\right)-\coth\left(\frac{\Theta_{s2}}{T}\right)\right)}}{2\left(c_2+c_2''\right)}. \quad (3)$$

Convention dictates that, in the absence of saturation effects, the order parameter for a displacive phase transition is set to a value of one at 0 K. On the other hand, increasing the value of T_{c2x} immediately causes q_4 to take on values greater than one. Maintaining the usual convention for all compositions can be achieved by rescaling q_4 to q_4/q_4', where q_4' is the value of q_4 at 0 K, without the influence of order parameter saturation, giving

$$\begin{aligned} G = {} & \frac{1}{2}a_2q_4'^2\Theta_{s2}\left(\coth\left(\frac{\Theta_{s2}}{T}\right)-\coth\left(\frac{\Theta_{s2}}{T_{c2x}}\right)\right)\left(\frac{q_4^2+q_5^2+q_6^2}{q_4'^2}\right)+\frac{1}{4}b_2q_4'^4\left(\frac{q_4^2+q_5^2+q_6^2}{q_4'^2}\right)^2 \\ & +\frac{1}{4}b_2'q_4'^4\left(\frac{q_4^4+q_5^4+q_6^4}{q_4'^4}\right)+\frac{1}{6}c_2q_4'^6\left(\frac{q_4^2+q_5^2+q_6^2}{q_4'^2}\right)^3+\frac{1}{6}c_2'q_4'^2\left(\frac{q_4q_5q_6}{q_4'}\right)^2 \\ & +\frac{1}{6}c_2''q_4'^6\left(\frac{q_4^2+q_5^2+q_6^2}{q_4'^2}\right)\left(\frac{q_4^4+q_5^4+q_6^4}{q_4'^4}\right)+\lambda_2q_4'^2e_a\left(\frac{q_4^2+q_5^2+q_6^2}{q_4'^2}\right) \\ & +\lambda_4q_4'^2\left[\sqrt{3}e_o\left(\frac{q_5^2-q_6^2}{q_4'^2}\right)+e_t\left(\frac{2q_4^2-q_5^2-q_6^2}{q_4'^2}\right)\right]+\lambda_5q_4'\left(\frac{e_4q_4q_6+e_5q_4q_5+e_6q_5q_6}{q_4'}\right) \\ & +\frac{1}{4}\left(C_{11}^o-C_{12}^o\right)\left(e_o^2+e_t^2\right)+\frac{1}{6}\left(C_{11}^o+2C_{12}^o\right)e_a^2+\frac{1}{2}C_{44}^o\left(e_4^2+e_5^2+e_6^2\right). \end{aligned} \quad (4)$$

In renormalized form for the $Pm\bar{3}m \leftrightarrow I4/mcm$ transition, this becomes

$$G = \frac{1}{2}a_2 q_4'^2 \Theta_{s2}\left(\coth\left(\frac{\Theta_{s2}}{T}\right) - \coth\left(\frac{\Theta_{s2}}{T_{c2x}}\right)\right)\left(\frac{q_4}{q_4'}\right)^2 + \frac{1}{4}\left(b_2^* + b_2'^*\right)q_4'^4\left(\frac{q_4}{q_4'}\right)^4 + \frac{1}{6}\left(c_2 + c_2''\right)q_4'^6\left(\frac{q_4}{q_4'}\right)^6. \quad (5)$$

The value of q_4' is itself given by

$$q_4'^2 = \frac{-\left(b_2^* + b_2'^*\right) + \sqrt{\left(b_2^* + b_2'^*\right)^2 + 4a_2\left(c_2 + c_2''\right)\left(T_{c2x} - T\right)}}{2\left(c_2 + c_2''\right)} \quad (6)$$

with $T = 0$. The equilibrium evolution of q_4/q_4' is given by

$$\left(\frac{q_4}{q_4'}\right)^2 = \frac{-\left(b_2^* + b_2'^*\right)q_4'^4 + \sqrt{\left(\left(b_2^* + b_2'^*\right)q_4'^4\right)^2 + 4a_2 q_4'^2\left(c_2 + c_2''\right)q_4'^6\Theta_{s2}\left(\coth\left(\frac{\Theta_{s2}}{T_{c2x}}\right) - \coth\left(\frac{\Theta_{s2}}{T}\right)\right)}}{2\left(c_2 + c_2''\right)q_4'^6}. \quad (7)$$

Expressions for the intrinsic elastic properties (i.e., excluding the effects of microstructure), obtained by following the same sequence of steps as set out in Carpenter (2007), are listed in Table 1. While this rescaling achieves the desired result of maintaining $q_4/q_4' \le 1$ at all compositions and temperatures, in practice the expressions for elastic constants in terms of q_4/q_4' (Table 1) give the same results as the expressions for the elastic constants in Table 2 of Carpenter (2007) when q_4 is allowed to exceed the value of one (Eqs. 1–3).

TABLE 1. Elastic constant variations expected in the stability field of a structure with *I4/mcm* symmetry ($q_4 \neq 0$, $q_5 = q_6 = 0$), due to a transition from a parent cubic structure with $Pm\bar{3}m$ symmetry, and taking into account the variation of composition

$C_{11} = C_{22} = C_{11}^o - M^2\chi_4\left(\frac{q_4}{q_4'}\right)^2$	$C_{13} = C_{23} = C_{12}^o - MN\chi_4\left(\frac{q_4}{q_4'}\right)^2$
$C_{33} = C_{11}^o - N^2\chi_4\left(\frac{q_4}{q_4'}\right)^2$	$C_{44} = C_{55} = C_{44}^o - \lambda_5^2 q_4^2\chi_6\left(\frac{q_4}{q_4'}\right)^2$
$C_{12} = C_{12}^o - M^2\chi_4\left(\frac{q_4}{q_4'}\right)^2$	$C_{66} = C_{66}^o$
* $K_V = \frac{1}{3}\left(C_{11}^o + 2C_{12}^o\right) - 4\lambda_2^2 q_4'^4\chi_4\left(\frac{q_4}{q_4'}\right)^2$	
* $G_V = \frac{1}{5}\left(C_{11}^o - C_{12}^o + 3C_{44}^o\right) - \frac{2}{5}\left(8\lambda_4^2 q_4'^4\chi_4 + \lambda_5^2 q_4'^2\chi_6\right)\left(\frac{q_4}{q_4'}\right)^2$	
† $\chi_4^{-1} = \frac{\partial^2 G}{\partial\left(q_4/q_4'\right)^2} = 2\left(b_2 + b_2'\right)q_4'^4\left(\frac{q_4}{q_4'}\right)^2 + 4\left(c_2 + c_2''\right)q_4'^6\left(\frac{q_4}{q_4'}\right)^4$	
† $\chi_6^{-1} = \partial^2 G/\partial q_6^2 = \left[\frac{12\lambda_4^2 q_4'^2}{\frac{1}{2}\left(C_{11}^o - C_{12}^o\right)} - b_2' q_4'^2\right]\left(\frac{q_4}{q_4'}\right)^2 - \frac{2}{3}c_2'' q_4'^4\left(\frac{q_4}{q_4'}\right)^4$	
$M = \left(2\lambda_2 - \frac{4}{\sqrt{3}}\lambda_4\right)q_4'^2$	$N = \left(2\lambda_2 + \frac{8}{\sqrt{3}}\lambda_4\right)q_4'^2$

Notes: The order parameter is scaled as $q_4/q_4' \le 1$, where q_4' is the value of q_4 at 0 K for the case of a system without saturation (Eq. 5).

* Expressions for the Voigt limits of bulk and shear modulus in terms of single-crystal elastic constants for a crystal with point group 4/*mmm* were taken from Watt and Peselnik (1980).

† Values of q_4/q_4' in the expressions for susceptibility are the equilibrium values given by Equation 7.

For hydrostatic pressure (P) as the external variable, the starting assumption is again that the Landau coefficients calibrated for $SrTiO_3$ as a function of temperature do not change. The main focus is on the pressure dependence of the critical temperature. Equation 41 of Carpenter (2007) can be used as

$$\begin{aligned} G = {} & \frac{1}{2}a_2\Theta_{s2}\left(\coth\left(\frac{\Theta_{s2}}{T}\right) - \coth\left(\frac{\Theta_{s2}}{T_{c2x}}\right)\right)\left(q_4^2 + q_5^2 + q_6^2\right) + \frac{1}{4}b_2\left(q_4^2 + q_5^2 + q_6^2\right)^2 \\ & + \frac{1}{4}b_2'\left(q_4^4 + q_5^4 + q_6^4\right) + \frac{1}{6}c_2\left(q_4^2 + q_5^2 + q_6^2\right)^3 + \frac{1}{6}c_2'\left(q_4 q_5 q_6\right)^2 \\ & + \frac{1}{6}c_2''\left(q_4^2 + q_5^2 + q_6^2\right)\left(q_4^4 + q_5^4 + q_6^4\right) + \lambda_2 e_a\left(q_4^2 + q_5^2 + q_6^2\right) \\ & + \lambda_4\left[\sqrt{3}e_o\left(q_5^2 - q_6^2\right) + e_t\left(2q_4^2 - q_5^2 - q_6^2\right)\right] + \lambda_5\left(e_4 q_4 q_6 + e_5 q_4 q_5 + e_6 q_5 q_6\right) \\ & + \frac{1}{4}\left(C_{11}^o - C_{12}^o\right)\left(e_o^2 + e_t^2\right) + \frac{1}{6}\left(C_{11}^o + 2C_{12}^o\right)e_a^2 + \frac{1}{2}C_{44}^o\left(e_4^2 + e_5^2 + e_6^2\right) \\ & + Pe_a. \end{aligned} \quad (8)$$

For a thermodynamically continuous transition, the transition pressure (P_c) is given by

$$P_c = \frac{a_2\Theta_{s2}\frac{1}{3}\left(C_{11}^o + 2C_{12}^o\right)}{2\lambda_2}\left(\coth\left(\frac{\Theta_{s2}}{T}\right) - \coth\left(\frac{\Theta_{s2}}{T_{c2x}}\right)\right). \quad (9)$$

If the volume strain continues to scale with q_4^2 as in Equation 6 of Carpenter (2007), i.e.,

$$e_a = -\frac{\lambda_2\left(q_4^2 + q_5^2 + q_6^2\right)}{\frac{1}{3}\left(C_{11}^o + 2C_{12}^o\right)}, \quad (10)$$

the renormalized form of Equation 8, with $q_4 \neq 0$, $q_5 = q_6 = 0$, can be written as

$$G = \frac{1}{2}\left(\frac{2\lambda_2}{\frac{1}{3}\left(C_{11}^o + 2C_{12}^o\right)}\right)\left(P_c - P\right)q_4^2 + \frac{1}{4}\left(b_2^* + b_2'^*\right)q_4^4 + \frac{1}{6}\left(c_2 + c_2''\right)q_4^6. \quad (11)$$

The solution for q_4 is then

$$q_4^2 = \frac{-\left(b_2^* + b_2'^*\right) + \sqrt{\left(b_2^* + b_2'^*\right)^2 + 4\frac{2\lambda_2}{\frac{1}{3}\left(C_{11}^o + 2C_{12}^o\right)}\left(c_2 + c_2''\right)\left(P - P_c\right)}}{2\left(c_2 + c_2''\right)}. \quad (12)$$

The inverse susceptibilities, χ_4^{-1} and χ_6^{-1}, and the elastic constants continue to depend on the order parameter according to the expressions given in Table 2 of Carpenter (2007). For composition as the external variable, Equation 4 yields an expression for χ_6^{-1} that is the same as that obtained from Equation 1. The expression for C_{44} also remains the same. The form of χ_4^{-1} is slightly different when q_4/q_4' is used in place of q_4 (see Table 1), but the q_4' terms cancel out in the expressions for C_{11}, C_{33}, C_{12}, and C_{13}.

(Ca,Sr)TiO_3 PHASE DIAGRAM

Given the importance assigned to the composition-dependence of T_{c2}, a phase diagram with well-constrained transition temperatures is a prerequisite for any analysis of the elastic prop-

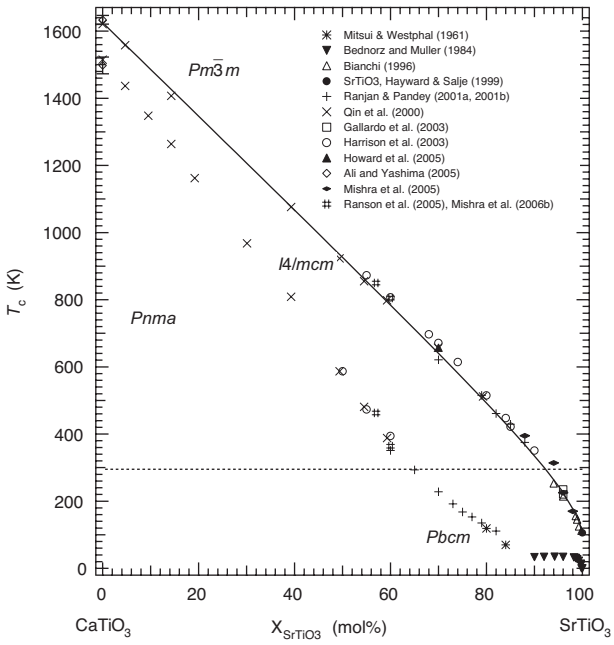

FIGURE 1. Summary of data from the literature for transition temperatures in the binary solid solution $CaTiO_3$-$SrTiO_3$. The transition temperatures of Ranjan and Pandey (2001b) and Ranjan et al. (2000) for a tetragonal ↔ orthorhombic transition just below the cubic ↔ tetragonal transition in the range ~65–90% $SrTiO_3$ are not included. Data of Bianchi (1996) are given in Lemanov (1997). The horizontal broken line represents room temperature. The solid curve is a fit to Equation 13. The tetragonal ↔ orthorhombic transitions occur across two-phase intervals spanning ~30–40 K (Mishra et al. 2006b), but these are not shown here.

erties of CST perovskites. A summary of transition temperature data from the literature is given in Figure 1. Until recently there was widespread agreement that the first transition during cooling from the stability field of the $Pm\bar{3}m$ structure is to the tetragonal *I*4/*mcm* structure (Cowley 1996; Redfern 1996; Lemanov 1997; Kennedy et al. 1999; Qin et al. 2000; Ranjan and Pandey 2001b; Harrison et al. 2003; Howard et al. 2005). This transition appears to be thermodynamically continuous at all compositions (Qin et al. 2000; Harrison et al. 2003), though it is close to tricritical in pure $CaTiO_3$ (Carpenter et al. 2001) and close to second order in pure $SrTiO_3$ (Salje et al. 1998; Hayward and Salje 1999). This means that T_{c2x} is the transition temperature as well as the critical temperature across the solid solution. At Ca-rich compositions, the next transition is first order in character, involving the symmetry change *I*4/*mcm* ↔ *Pnma* (Redfern 1996; Qin et al. 2000; Carpenter et al. 2001; Harrison et al. 2003; Ali and Yashima 2005). For Sr-rich compositions Ranjan and Pandey (1999) and Ranjan et al. (1999, 2000) proposed that an orthorhombic structure becomes stable a few degrees below the cubic ↔ tetragonal transition temperatures. They claimed that this was the *I*4/*mcm* ↔ *Pnma* transition, but subsequently suggested that their orthorhombic phase might alternatively have *Imma* symmetry (Ranjan and Pandey 2001b; Ranjan et al. 2001; Mishra et al. 2002). This contradicts the conclusions of Mitsui and Westphal (1961), Ball et al. (1998), Qin et al. (2000, 2002), Yamanaka et al. (2002), and Howard et al. (2005) that the *I*4/*mcm* structure is stable at room temperature in this composition range. Yamanaka et al. (2002) obtained single-crystal diffraction evidence for *I*4/*mcm* symmetry at composition CST65, while the other studies were based on powder diffraction spectra. Note, however, that the pseudocubic lattice parameters for this sample are more like those of Mishra et al. (2006a) for the *Pbcm* structure than those of Ball et al. (1998) for the tetragonal structure. More recently, Ranson et al. (2005) and Mishra et al. (2005, 2006a, 2006b) have argued that the first transition in the range CST64–CST95 is to an orthorhombic (pseudotetragonal) structure with *Imma* symmetry. A $Pm\bar{3}m$ ↔ *Imma* transition is required by symmetry to be first order in character, however (Howard and Stokes 1998), and Mishra et al. (2006b) found no detectable differences in the evolution of lattice geometry with temperature for samples, which were purported to show $Pm\bar{3}m$ ↔ *I*4/*mcm* (CST57) and $Pm\bar{3}m$ ↔ *Imma* (CST60) transitions. Ball et al. (1998) originally claimed that crystals with compositions close to CST50, which have pseudocubic lattice geometry, actually have *Cmcm* symmetry. Subsequent analysis has shown that the correct space group for these is *Pnma* (Howard et al. 2001; Ranjan et al. 2001). In the present study, the transition sequence is treated as being $Pm\bar{3}m$ ↔ *I*4/*mcm* ↔ *Pnma* with increasing $CaTiO_3$ content at room temperature, where the boundaries occur in the vicinity of ~8% $CaTiO_3$ (CST92) and ~36% $CaTiO_3$ (CST64) (Fig. 1). In the composition range CST60–CST64, the orthorhombic structure is in fact believed to have space group *Pbcm* (Mishra et al. 2006a), but an analysis of the elastic behavior of this phase is beyond the scope of the present study. No evidence has been found in lattice geometry for the monoclinic structures with space groups $P2_1/m$ and $C2/m$ proposed by Woodward et al. (2006).

Further phase transitions occur below room temperature. Mitsui and Westphal (1961) found evidence, from a dielectric anomaly and from X-ray diffraction, for a transition at ~116 and ~70 K in CST80 and CST84, respectively. Ranjan and Pandey (2001a) mapped the same dielectric anomaly as a function of composition and temperature. They obtained a trend that meets up with the trend for the *I*4/*mcm* ↔ *Pnma* transition from high temperatures, though with a different slope (Fig. 1). Ranjan et al. (2000) and Mishra et al. (2002, 2006b) proposed that the low symmetry phase at this transition has space group *Pbcm*. Below ~35 K, the trend of transition temperatures changes again for the most Sr-rich compositions (Bednorz and Müller 1984), but this low-temperature behavior is not directly relevant to the present study.

A description of the $Pm\bar{3}m$ ↔ *I*4/*mcm* transition line is required for the Landau analysis given below. Various expressions might be fit to the data for the transition temperature as a function of composition, T_{c2x}, more or less arbitrarily. The significant non-linearity at Sr-rich compositions is, however, strongly reminiscent of the curvature due to saturation effects at low temperatures. Hayward and Salje (1998) have shown that order parameter saturation causes the transition line for a thermodynamically continuous transition to asymptote to 0 K according to

$$T_{cx} = \frac{\Theta_s}{\coth^{-1}\left(\coth\left(\frac{\Theta_s}{T_c}\right) - kx\right)}, \quad (13)$$

where x represents composition in mol% of $SrTiO_3$, k is a constant, and T_c represents the transition temperature for a sample whose composition is specified by $x = 0$. In the case of (Ca,Sr)TiO_3, the transition temperature never reaches zero but it does fall off non-linearly at low temperatures for the most $SrTiO_3$-rich compositions. A first fit of Equation 13 to all the data gave $\Theta_s = 274$ K, $T_c = 1621$ K, $k = 0.05$ (with composition expressed in mol% as $x = 0$ for pure $CaTiO_3$ and $x = 100$ for pure $SrTiO_3$). Constraining the fit so that the transition temperature of $SrTiO_3$ is more nearly equal to 106 K gave the curve shown in Figure 1, which has $\Theta_s = 258$ K, $T_c = 1625$ K, $k = 0.053$. In principle, the saturation temperature should be the same as found for order parameter saturation at low temperatures in pure $SrTiO_3$, i.e., 60.8 K (Hayward and Salje 1999). However, the much higher value extracted from the T_c variations must include effects due to overlapping strain fields around impurity Ca atoms at the dilute limit of the solid solution, as occurs in other systems (Salje et al. 1991; Hayward and Salje 1996; Redfern and Schofield 1996). The disparity suggests that such strain effects are more important in determining the curvature of T_c than straightforward order parameter saturation. For present purposes, Equation 1 appears to provide a satisfactory description of the composition dependence of the $Pm\bar{3}m \leftrightarrow I4/mcm$ transition temperature.

Volume strains for the cubic ↔ tetragonal transition in CST are negative (Carpenter et al. 2001; Carpenter 2007). Increasing pressure should therefore cause a lowering of symmetry for Sr-rich samples with $Pm\bar{3}m$ or $I4/mcm$ symmetry at ambient conditions. The transition pressures at room temperature are not as tightly constrained as the transition temperatures at room pressure. For $SrTiO_3$, the most carefully defined value of transition pressure, P_c, for the $Pm\bar{3}m \leftrightarrow I4/mcm$ transition is 6.4 GPa (Ishidate and Isonuma 1992). This compares with earlier determinations of 6.5 GPa (Ishidate et al. 1988) and 6 GPa (Bonello et al. 1989a, 1989b; Fischer et al. 1989) and a later determination of 6.0 GPa by Grzechnik et al. (1997). The data of Carpenter et al. (2007) for elastic softening are consistent with a transition pressure of ~2.0 GPa for CST95. In pressure-composition space, this falls between the value of P_c for $SrTiO_3$ and the critical composition of ~92% $SrTiO_3$ (Fig. 2). Equation 9, with values of the coefficients taken from Carpenter (2007) and values of T_{c2x} from the fit to Equation 13, has been used to calculate the $Pm\bar{3}m \leftrightarrow I4/mcm$ transition pressure as a function of composition (solid line in Fig. 2).

Yamanaka et al. (2002) reported that CST65 has a primitive orthorhombic structure at 3.5 GPa and proposed *Pnma* symmetry, with the tetragonal ↔ orthorhombic transition occurring between this point and ambient pressure. However, Carpenter et al. (2007) observed changes in slope of elastic properties as a function of pressure in the vicinity of ~3 GPa for a polycrystalline sample with the same nominal composition, but did not observe any discontinuities that might indicate a discrete phase transition. At ambient conditions the $I4/mcm \leftrightarrow Pbcm$ boundary occurs between CST64 and CST65, and the $Pbcm \leftrightarrow Pnma$ boundary between CST59 and CST60 (Ranjan et al. 2001; Ranson et al. 2005; Mishra et al. 2006a). It is not clear whether these points can be linked to the peak splitting in Raman spectra from $SrTiO_3$ observed by Grzechnik et al. (1997) at 15.5 GPa, which might be understood in terms of a transition to orthorhombic symmetry.

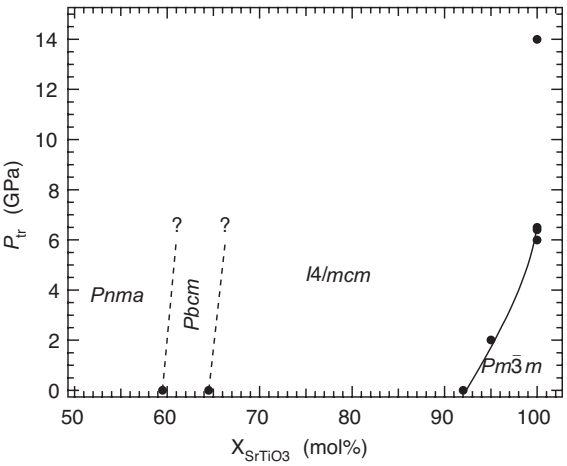

FIGURE 2. Transition pressures as a function of composition at room temperature. The composition at which the $Pm\bar{3}m \leftrightarrow I4/mcm$ transition occurs at ambient conditions is taken from Figure 1. Approximate composition limits for the *Pbcm* structure at ambient conditions are from Mishra et al. (2006a). Data for the $Pm\bar{3}m \leftrightarrow I4/mcm$ transition in $SrTiO_3$ are from Ishidate and Isonuma (1992), Bonello et al. (1989a, 1989b), and Grzechnik et al. (2002). The solid line is the calculated transition pressure (Eq. 9). The data point for CST95 is from Carpenter et al. (2007) . The possible tetragonal ↔ orthorhombic transition reported by Grzechnik et al. (1997) to be between ~12 and ~15 GPa is shown arbitrarily at 14 GPa. Broken lines are arbitrary placements of trends for $I4/mcm \leftrightarrow Pbcm$ and $Pbcm \leftrightarrow Pnma$ transitions.

CALIBRATION OF COMPOSITION-DEPENDENT PARAMETERS

Having developed functional forms for elastic constant variations with composition and a complete calibration for pure $SrTiO_3$, the central issue for characterizing the effect of strain/order parameter coupling on elasticity changes across the CST solid solution is the extent to which values of the coefficients themselves depend on composition. The bare elastic constants will certainly vary to some extent with composition but, to a first approximation, can probably be regarded as constant. If the soft mode mechanism for the cubic ↔ tetragonal transition is essentially the same for $CaTiO_3$ as it is for $SrTiO_3$, then values of the a, b_2, b_2', c_2, and c_2'' coefficients will also be more or less constant across the solid solution. (It is unlikely that Θ_s is independent of composition, but this becomes a relevant factor only below room temperature). On the other hand, the thermodynamic character of this transition changes from close to tricritical in $CaTiO_3$ (Carpenter et al. 2001) to close to second order in $SrTiO_3$ (Salje et al. 1998; Hayward and Salje 1999). This implies that the sum of the renormalized fourth order coefficients, $(b_2^* + b_2'^*)$, is not constant. Since these coefficients depend on the strain/order parameter coupling coefficients according to

$$\left(b_2^* + b_2'^*\right) = b_2 + b_2' - \frac{2\lambda_2^2}{\frac{1}{3}\left(C_{11}^o + 2C_{12}^o\right)} - \frac{8\lambda_4^2}{\frac{1}{2}\left(C_{11}^o - C_{12}^o\right)}, \quad (14)$$

(from Eqs. 13 and 14 of Carpenter 2007), the simplest model for the solid solution can be reduced to one in which only T_{c2x} and λ_4 are

allowed to vary. This is easily tested by comparing observed and calculated variations of the tetragonal strain, e_t, which is expected to follow the order parameter according to

$$e_t = -\frac{2\lambda_4 q_4^2}{\frac{1}{2}\left(C_{11}^o - C_{12}^o\right)}. \quad (15)$$

Setting $b_2^* + b'^*_2 = 0$ for $CaTiO_3$ requires $\lambda_4 = -0.131$ if λ_2 is kept at the value extracted for $SrTiO_3$ (0.046), the bare elastic constants of $SrTiO_3$ are retained and conversion between units of GPa and J·mol^{-1} is achieved using the same molar volume as given for $SrTiO_3$ in Carpenter (2007). The resulting variations of e_t for $CaTiO_3$ shown in Figure 3a have been calculated using values of the coefficients listed in Table 6 of Carpenter (2007), with $T_{c2x} = 1625$ K. They are in semi-quantitative agreement with the observed variations of e_t from Carpenter et al. (2001) if the temperature scale of the original experimental data of Kennedy et al. (1999) is adjusted upward to match the revised value of T_c. A constant value of λ_2 does not produce as close a match between the observed and calculated volume strain, e_a, which is expected to scale with the order parameter as

$$e_a = -\frac{\lambda_2 q_4^2}{\frac{1}{3}\left(C_{11}^o + 2C_{12}^o\right)}. \quad (16)$$

The value of λ_2 should probably also be allowed to vary with composition, therefore, but the data for e_a of $CaTiO_3$ are poorly constrained due to the uncertainties of defining and extrapolating a lattice parameter for the cubic reference structure from only four data points (Carpenter et al. 2001).

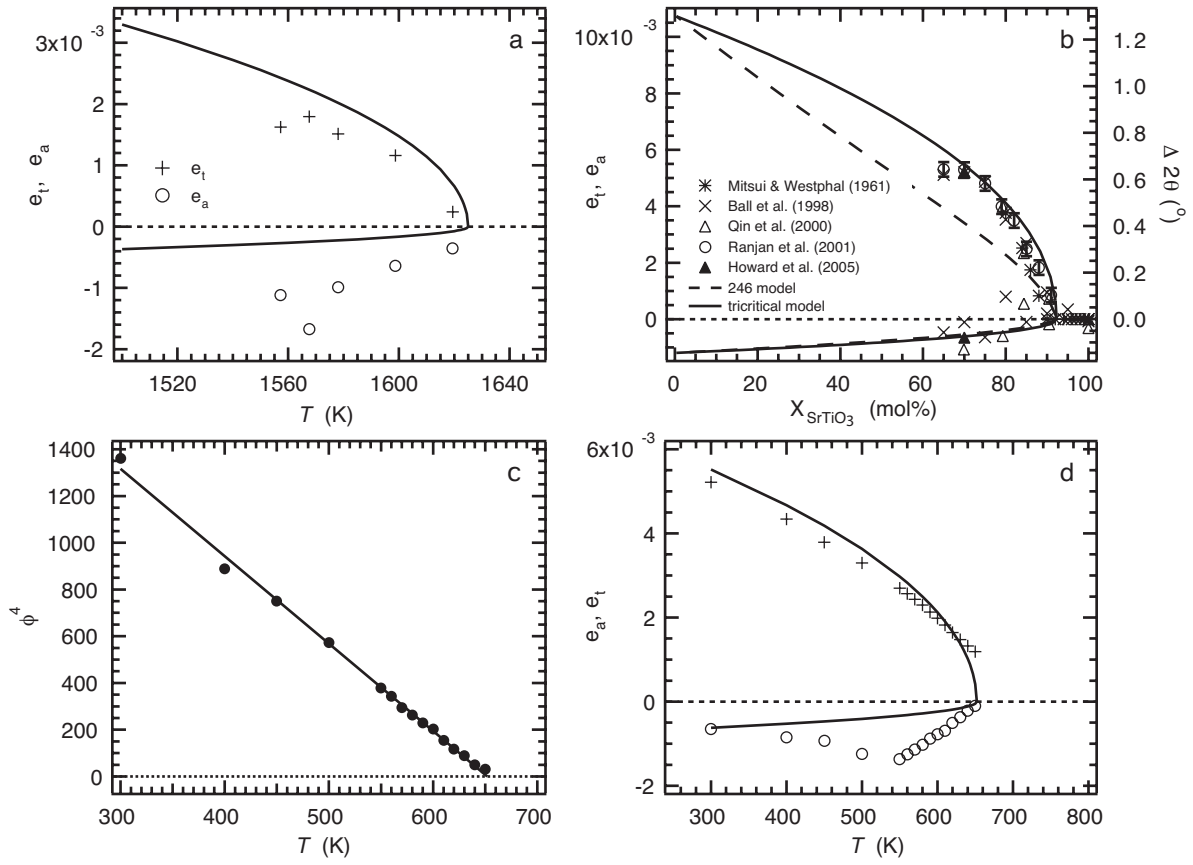

FIGURE 3. (**a**) Data points represent variations of the tetragonal strain, e_t, and volume strains, e_a, of $CaTiO_3$ taken from Carpenter et al. (2001). They were extracted from lattice parameter data of Kennedy et al. (1999). The original temperatures given by Kennedy et al. have been rescaled upward to be consistent with a transition temperature of 1625 K. Curves are calculated variations of e_t and e_a for a tricritical model with $\lambda_4 = -0.131$ GPa, $T_c = 1625$ K, and other parameters taken from the calibration for $SrTiO_3$. (**b**) Data points are experimental values of the tetragonal and volume strains at room temperature, as extracted by Carpenter et al. (2001) from published lattice parameters. Values of e_t and e_a at room temperature have been extracted from lattice parameter data for CST70 of Howard et al. (2005). Data points of Ranjan et al. (2001) refer to the right-hand axis and are experimental values for the splitting between 004 and 400/040 reflections in powder X-ray diffraction patterns. The right hand axis has been scaled so that e_t and $\Delta 2\theta$ values overlap. Solid and broken lines are calculated variations of e_t and e_a at 295 K for tricritical and 246 models of the solid solution, respectively. (**c**) The octahedral tilt angle, ϕ (in degrees), for tetragonal CST70 from Howard et al. (2005) varies as $\varphi^4 \propto T$, to a good approximation, giving $T_c = 652$ K. This is consistent with tricritical character for the cubic-tetragonal transition (Howard et al. 2005). (**d**) Variations of e_t extracted from the lattice parameter data of Howard et al. (2005) for CST70 (crosses) are also consistent with variations calculated using the tricritical model (solid line: $\lambda_4 = -0.131$ GPa, $T_c = 652$ K and all other parameters as for $SrTiO_3$). Agreement between observed (circles) and calculated values of e_a is not as close, but the experimental data are subject to a large uncertainty associated with extrapolating the cubic lattice parameter from high temperatures into the stability field of the tetragonal structure.

Variations of the tetragonal strains and volume strains as a function of composition at 295 K are shown in Figure 3b. These were taken from Carpenter et al. (2001), as extracted from original lattice parameter data of Mitsui and Westphal (1961), Ball et al. (1998), and Qin et al. (2000). Strains determined from lattice parameters of Howard et al. (2005) for CST70 are in close agreement. Ranjan et al. (2001) have given values of the angle, $\Delta 2\theta$, between 004 and 400/040 peaks in powder diffraction patterns for Sr-rich samples with a range of compositions, and these are expected to be linear with e_t. With appropriate scaling (right axis, Fig. 3b), they indeed overlap with the tetragonal strain data and provide tight constraints on how the tetragonal structure evolves with increasing $CaTiO_3$ content. Assuming that λ_4 varies linearly with composition between –0.131 for $CaTiO_3$ and –0.075 for $SrTiO_3$, but with all other coefficients taken from $SrTiO_3$, and that the variation of T_{c2x} is specified by the fit of Equation 13, leads to the calculated variation for e_t as a function of composition at 295 K. Agreement with the observed variations (broken line in Fig. 3b) is poor and an alternative model seems justified. If it is assumed that λ_4 varies rapidly over a narrow composition interval at Sr-rich compositions and that the $Pm\bar{3}m \leftrightarrow I4/mcm$ transition is tricritical for all compositions with $T_c > 295$ K, much better agreement is obtained between the observed and calculated variations of e_t (solid line in Fig. 3b). In this model, $\lambda_4 = -0.131$ GPa and $b_2^* + b_2'^* = 0$ for compositions between CST0 and CST92. The volume strain is small, and calculated variations are at least consistent with the rather scattered data. These two different descriptions are referred to below as 246 and tricritical models, respectively. Data from Howard et al. (2005) for CST70 as a function of temperature are also consistent with the tricritical model. The octahedral tilt angle, φ, varies as $\varphi^4 \propto T$ (Howard et al. 2005; Fig. 3c), with $T_c = 652$ K. Calculated variations of e_t and e_a, using the parameters of $SrTiO_3$ and $\lambda_4 = -0.131$, are compared with observed variations in Figure 3d. The volume strains are subject to a large uncertainty due to their dependence on extrapolated values of the cubic lattice parameters from only three data points above T_c, but the model variation of e_t is in close agreement with the observed variation.

An additional test of simple models for the complete solid solution is to compare observed and calculated excess enthalpies or entropies for the cubic ↔ tetragonal transition. Guyot et al. (1993) measured the heat capacity of $CaTiO_3$ at high temperatures by drop-calorimetry. Their raw data for relative enthalpy, H_T-H_{273}, are reproduced in Figure 4a. The excess enthalpy due to transitions from the cubic parent structure is given by differences between observed values and values for the cubic structure extrapolated from high temperatures. A linear fit to the highest temperature data is adequate for a short extrapolation and leads to the excess enthalpies shown in Figure 4b. The excess enthalpy due to a tricritical $Pm\bar{3}m \leftrightarrow I4/mcm$ transition is (for T_c, $T >> \Theta_s$)

$$H = -\frac{1}{2}a_2 T_c q_4^2 + \frac{1}{6}\left(c_2 + c_2''\right)q_4^6. \quad (17)$$

This gives values that agree with the experimental data (Fig. 4b), though the closeness of the match may be fortuitous. The transition at 1621 K (Qin et al. 2000) was missed by Guyot et al. (1993), presumably because the enthalpy changes associated with it are small and continuous. An obvious discontinuity in the excess enthalpy between 1517 and 1541 K in Figure 4b is consistent with the first order transition temperature of 1520 K extracted from the same data by Guyot et al. (1993) and with the independently determined value of 1515 K reported by Qin et al. (2000). A further transition at 1384 K reported by Guyot et al. is not so clear in the interpretation of their data represented by Figure 4b.

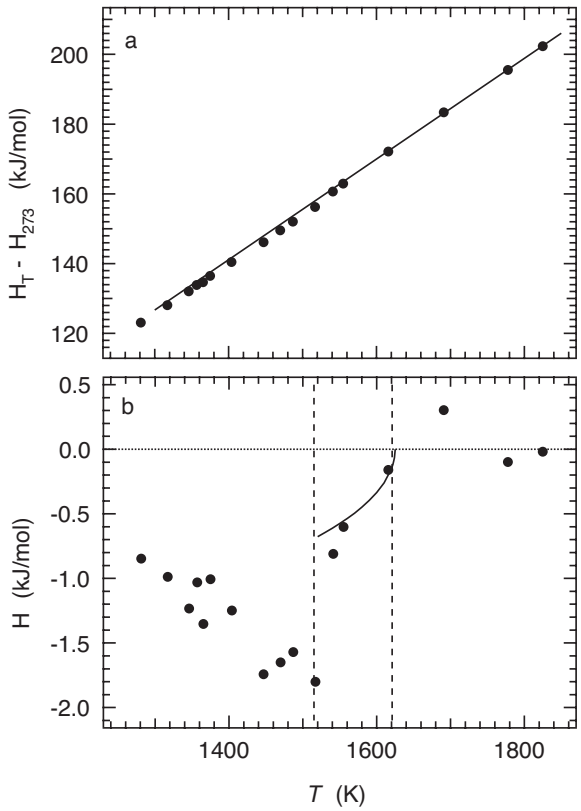

FIGURE 4. (**a**) Relative enthalpy data of Guyot et al. (1993) for $CaTiO_3$, as obtained by drop calorimetry. The straight line was fit to the four highest temperature data points and represents the relative enthalpy of cubic $CaTiO_3$. (**b**) Excess enthalpy from **a**, defined as the difference between experimental values and the straight line fit for cubic $CaTiO_3$. Broken lines mark the $Pm\bar{3}m \leftrightarrow I4/mcm$ and $I4/mcm \leftrightarrow Pnma$ transition temperatures given by Qin et al. (2000). A curve represents the excess enthalpy associated with the $Pm\bar{3}m \leftrightarrow I4/mcm$ transition, as calculated using Equation 17 and coefficients extracted for $SrTiO_3$, with $T_c = 1625$ K, $b_2^* + b_2'^* = 0$ (tricritical). Guyot et al. (1993) suggested that a further transition occurs at 1384 K, but this is not obvious from their data when presented in the form of excess enthalpy.

Heat capacity data for a sample with composition CST49 are reproduced from Qin et al. (2000) in Figure 5a. Standard analysis of the excess entropy (as for $SrTiO_3$ in Salje et al. 1998, for example) requires the fitting of a baseline to data for the high symmetry phase and extrapolation of this to lower temperatures. Irregularities in the C_P curve suggest that some drift of the instrumental baseline occurred during data collection, so that the analysis given here is subject to relatively large uncertainties. A linear baseline was fit to data in the temperature range 961–1004 K. The excess heat capacity, ΔC_P, due to the cubic ↔ tetragonal

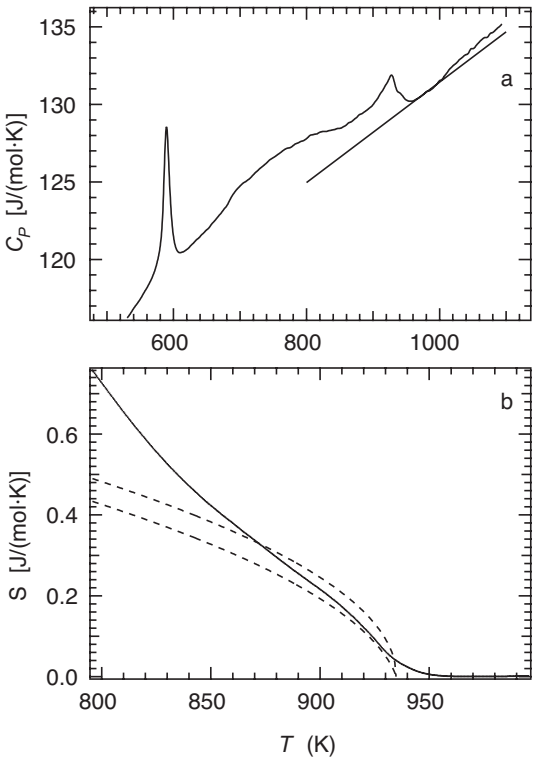

FIGURE 5. Heat capacity data for CST49, from Qin et al. (2000). The linear baseline was fit to data for the cubic phase just above the cubic ↔ tetragonal transition temperature, and was used to determine the excess heat capacity associated with the $Pm\bar{3}m \leftrightarrow I4/mcm$ transition. (**b**) Excess entropy calculated from the excess heat capacity taken from **a**. Broken lines are calculated variations for the tricritical model (upper curve) and the 246 model (lower curve) of the solid solution. Note that the experimental values (solid lines) are highly sensitive to the choice of baseline in **a**.

transition was taken as the difference between observed C_P values and the extrapolated baseline, and $\Delta C_P/T$ was then integrated to give the excess entropy, S, as a function of temperature. For T_c, $T >> \Theta_s$, the excess entropy in Equation 1 is given by

$$S = -\frac{1}{2} a q_4^2, \tag{18}$$

which was calculated using the same coefficients as before, with T_{c2x} = 935 K and values of λ_4, $b_2^* + b'^*_2$ from the 246 model. Both observed and calculated excess entropies are shown in Figure 5b. Excess entropies for the equally simple tricritical model, with λ_4 = –0.131 GPa across the solid solution, are also shown. The experimental values can only be treated seriously over a limited temperature interval below T_c and, in this range, both models provide a semi-quantitative description of the data.

A definitive calibration of the effects of solid solution will require higher resolution data for the heat capacity and spontaneous strains as a function of temperature at several different compositions within the solid solution.

PREDICTION OF ELASTIC CONSTANT VARIATIONS

Determinations of the Landau coefficients for $SrTiO_3$, together with the two simple models for the effects of solid solution, allow the prediction of anomalies in the elastic constants that accompany the $Pm\bar{3}m \leftrightarrow I4/mcm$ transition at any composition. These are shown for 295 K in Figure 6. In both models, the bulk modulus (K) is relatively insensitive to composition. Significant discontinuities are expected, however, in both the individual elastic constants and the shear modulus (G) of a polycrystalline sample at the critical composition of ~92% $SrTiO_3$. The main difference in elastic behavior between the two models is the curvature of single-crystal and bulk elastic constants as the cubic stability field is approached from the tetragonal side. Some softening is expected in cubic samples as their composition approaches the stability field of the tetragonal structure, but this has not been determined. For later comparisons with experimental data, the isotropic Young's modulus (E) has also been calculated. This is related to the bulk and shear moduli by

$$E = \frac{9KG}{3K + G} \tag{19}$$

A quantitative description of the (first order) $I4/mcm \leftrightarrow Pnma$ transition has not yet been developed, but the transition point should be marked by discontinuities in all the elastic constants. Expressions for Voigt limits of the shear modulus for *Pnma* structures from Carpenter (2007),

$$K_V = \frac{1}{3}\left(C_{11}^o + 2C_{12}^o\right) - 4\lambda_1^2\chi_2 q_2^2 - 8\lambda_2^2\chi_4 q_4^2 \tag{20}$$

$$G_V = \frac{1}{5}\left(C_{11}^o - C_{12}^o + 3C_{44}^o\right) - \frac{2}{5}\left(8\lambda_3^2\chi_2 + 3\lambda_6 + 2\lambda_7\right)q_2^2 - \frac{2}{5}\left(16\lambda_4^2\chi_4 + \lambda_5^2\chi_4 + \lambda_5^2\chi_5\right)q_4^2 \tag{21}$$

allow a qualitative prediction of bulk properties. Any change in bulk modulus is expected to be small because the volume strain remains small in the *Pnma* structure. The step in G at the transition point will be sensitive to the magnitude and sign of the coupling coefficients, λ_6 and λ_7.

The pressure dependences of the elastic constants of tetragonal $SrTiO_3$ have been calculated in the same way as described by Ishidate et al. (1988), but with a revised set of Landau coefficients and including sixth order terms. P_c is 6.41 GPa for pure $SrTiO_3$ at 295 K if the coefficients from Table 6 of Carpenter (2007) are substituted into Equation 9. Equation 12 gives the equilibrium evolution of q_4 in the $I4/mcm$ stability field and the susceptibilities χ_4^{-1}, χ_6^{-1} are given by the expressions in Table 2 of Carpenter (2007). The amount of softening was first determined for fixed values of C_{11}^o, C_{12}^o, C_{44}^o, and this was then subtracted from values of the elastic constants of cubic $SrTiO_3$ extrapolated to $P > P_c$. The pressure dependences of cubic elastic constants were measured up to 2 GPa by Beattie and Samara (1971), using pulse-echo ultrasonics, and by Ishidate et al. (1988) through the phase transition, using Brillouin scattering. The data of Ishidate et al. (1988) are reproduced in Figure 7a, and their linear fits for the cubic structure were used for the extrapolation to high pressures. Ishidate et al. (1988) reported that their sample remained free of twins in the stability field of the tetragonal structure and that they measured C_{11}, ½($C_{11} - C_{12}$), and C_{66} of this phase. Agreement between observed and calculated values of C_{11} and C_{66} (= C_{44}^o) is close (Fig. 7a). Note that ½($C_{11} - C_{12}$) is not expected to show any

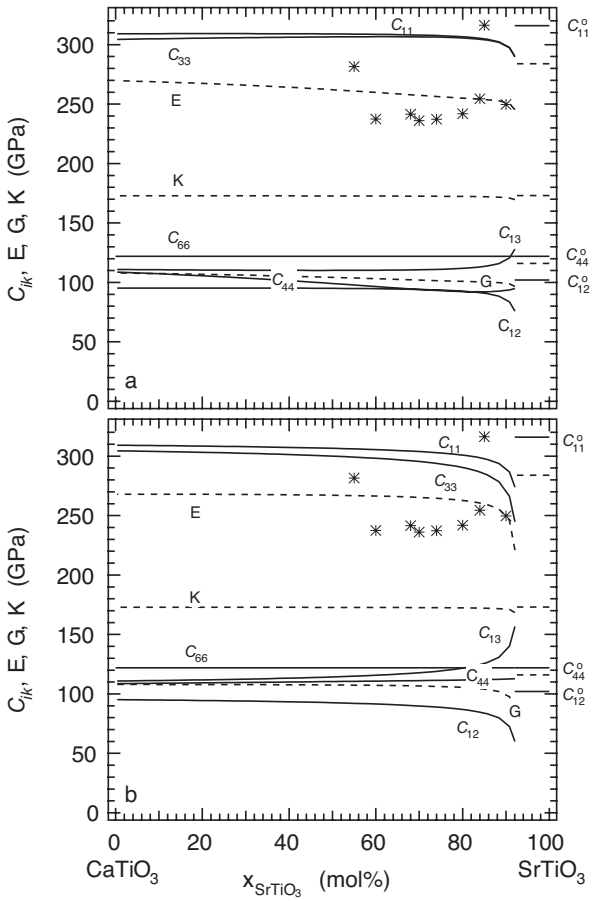

FIGURE 6. Predicted variations of single crystal (solid lines) and polycrystal (broken lines) elastic constants due to the $Pm\bar{3}m \leftrightarrow I4/mcm$ transition as a function of composition across the CST solid solution at 295 K. Values of cubic elastic constants (CST92–CST100) were taken from the fits to C_{11}, C_{12}, and C_{44} of cubic $SrTiO_3$ given in Carpenter (2007): $C_{11} = 316$, $C_{12} = 102$, $C_{44} = 122$ GPa at 295 K. Softening in the range CST0–CST92 due to the transition at CST92 was calculated using the expressions listed in Table 2 of Carpenter (2007) and values of the coefficients listed in Table 6 of Carpenter (2007), with transition temperatures given by Equation 13. For **a**, the value of λ_4 varied linearly with composition from –0.075 at CST100 to –0.131 at CST0 (246 model). For **b**, λ_4 was set at –0.131 for CST0–CST92 (tricritical model). Bulk (K) and shear (G) moduli are averages of the Reuss and Voigt limits calculated from the single-crystal elastic constants; the isotropic Young's modulus, E, was calculated from these. Stars are room temperature values of E extracted from the experimental data of Harrison et al. (2003) for polycrystalline samples with different compositions. They were converted from the relative values given by Harrison et al. (2003) to absolute values using values of E for cubic $SrTiO_3$ extrapolated to high temperatures.

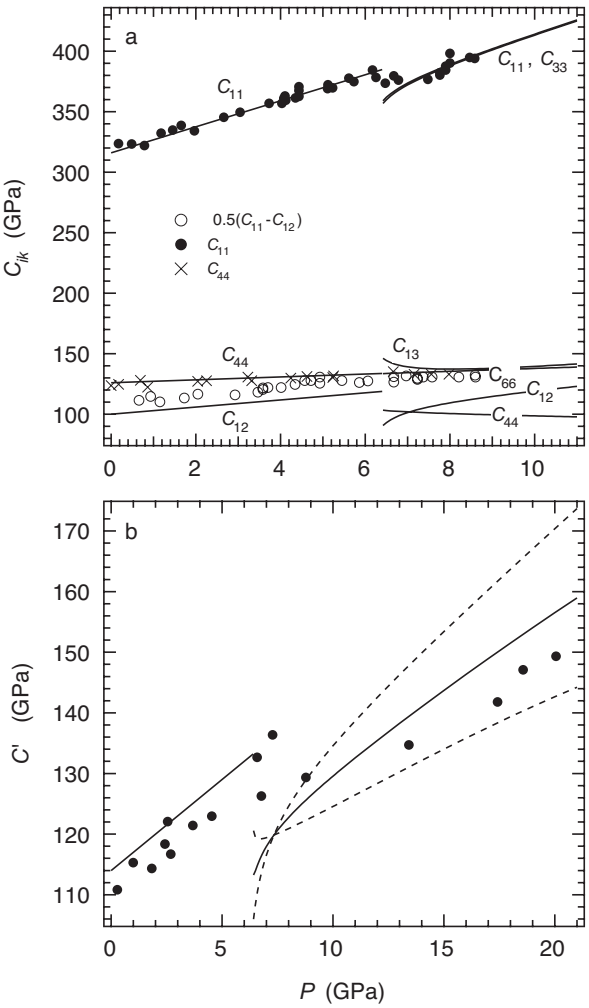

FIGURE 7. Calculated (curves) and observed (data points) variations of single-crystal elastic constants for $SrTiO_3$ as a function of pressure at room temperature. (**a**) Experimental data of Ishidate et al. (1988). Calculated variations of C_{11}, C_{12}, and C_{44} for cubic $SrTiO_3$ are from the fits to experimental data given by Ishidate et al. (**b**) Experimental data for the effective elastic constant, C', determining the velocity of a degenerate transverse acoustic mode traveling parallel to [111], from Fischer et al. (1989). In the stability field of the cubic phase $C' = 1/3 (C_{11} - C_{12} + C_{44})$. The calculated variation for cubic $SrTiO_3$ is given by the linear fits for C_{11}, C_{12}, C_{44} given by Ishidate et al. (1988), as shown in **a**. In the stability field of the tetragonal phase, the transverse acoustic wave is no longer degenerate, and the solid line is the average of the limiting values of C' calculated for two pure transverse modes (broken lines), using expressions given by Brugger (1965).

deviation through the transition pressure. Ishidate and Isonuma (1992) measured soft mode frequencies in the tetragonal stability field and found a value of 0.16 for the ratio of the squares of the frequencies for the E_g and A_{1g} modes, ω_E^2/ω_A^2. This compares with 0.12 and 0.14 for observed and calculated values at the temperature-driven transition (Carpenter 2007).

Brillouin data for a transverse acoustic wave propagating parallel to [111] have also been reported for $SrTiO_3$ as a function of pressure by Fischer et al. (1989) and were reproduced in Bonello et al. (1989a, 1989b). Their data are shown in Figure 7b along with the calculated variations obtained by combining the results shown in Figure 7a. They did not specify the microstructure of their single crystal at high pressures or the polarization directions of the acoustic mode they measured. For the cubic structure, the elastic constant combination relevant for the degenerate transverse acoustic mode parallel to [111] is $1/3(C_{11} - C_{12} + C_{44})$ and this was calculated using the fit parameters from

the data of Ishidate et al. (1988). In the tetragonal structure, there are two pure transverse modes with propagation direction parallel to [111] of the tetragonal structure. Expressions for the elastic constant combinations for these are given by Brugger (1965) and have been used to calculate the numerical values shown in Figure 7b. (The tetragonal distortion of $SrTiO_3$ is small so $[111]_{tetragonal}$ remains close to $[111]_{cubic}$.) The data for cubic $SrTiO_3$ derived from the data of Ishidate et al. are ~5% larger than the observed values from Fischer et al. (1989), but the calculated pattern of variations is similar to the observed pattern. At high pressures in the tetragonal stability field, the observed values of Fischer et al. (1989) lie between the limiting values calculated for the two pure transverse modes.

Finally, predicted variations of the bulk and shear moduli for polycrystalline $SrTiO_3$ are shown in Figure 8. The characteristic features of these are, once again, the small anomaly in *K* and a sharp discontinuity in *G*. The present author was not able to find in the literature any determination of these properties directly from a polycrystalline sample.

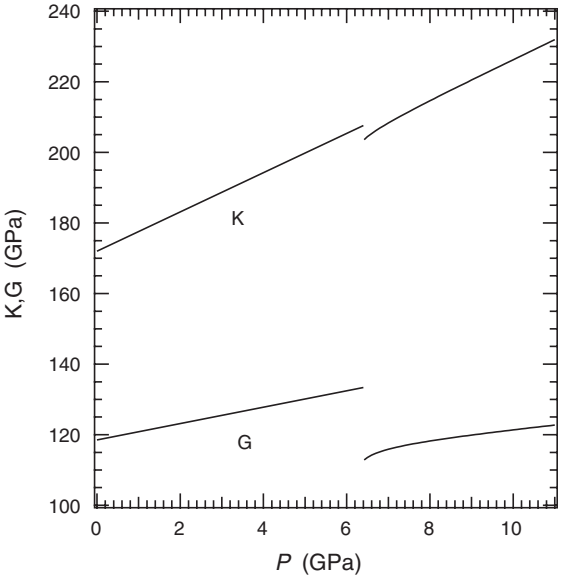

FIGURE 8. Calculated variations of bulk and shear moduli of polycrystalline $SrTiO_3$ as a function of pressure at 295 K. These are average values of Voigt and Reuss limits, calculated from the variations of single-crystal elastic constants shown in Figure 7a.

THE INFLUENCE OF TRANSFORMATION TWINS

It was recognized from the early days of elastic constant measurements on $SrTiO_3$ that the movement of twin walls can give rise to additional softening effects (Rehwald 1971; Fossheim and Berre 1972). This softening was seen in ultrasonic experiments, implying that twin walls are able to move on the time scale of applied stresses that operate at MHz frequencies. Single-crystal elastic constant data from the literature (Rehwald 1970; Lei 1991) suggest that the softening due to effects other than classical strain/order parameter coupling occurs only in the shear modulus (Fig. 9). C_{44} shows very little scatter between Brillouin measurements from within a single domain and ultrasonic measurements on polydomain samples and, in addition, C_{66} is not affected by the transition (see summary of data in Fig. 3 of Carpenter 2007). This means that softening is indeed restricted to shear elastic constants that are related to stresses that could drive twin wall displacements. Data for the isotropic Young's modulus derived from the same single-crystal ultrasonic data show that there is a softening of ~5–10% beyond the values calculated for strain/order parameter coupling in $SrTiO_3$ (Fig. 9). At frequencies of ~1–25 Hz, the softening influence of twin walls is substantially greater than this in polycrystalline samples from the CST solid solution held at high temperatures (Harrison et al. 2003) and in single crystals of $SrTiO_3$ at low temperatures (Schranz et al. 1999; Kityk et al. 2000a, 2000b; Binder and Knorr 2001; Lemanov et al. 2002). With the new calibrations for $SrTiO_3$ (Carpenter 2007) and the models for CST presented above, it is now possible to separate the lattice contributions, i.e., the strain/order parameter coupling, from domain wall effects quantitatively.

Models for softening due to twin wall mobility

Whereas softening due to strain coupling depends on the order parameter susceptibility, softening due to twin wall motions can be treated as an excess property related to the spontaneous strain. Following Schranz et al. (1999) and Kityk et al. (2000a, 2000b), this is expressed more conveniently in terms of elastic compliances (S_{ik}) than in terms of the elastic constants (C_{ik}). In general terms, the compliance, S_{FE}, for a ferroelastic crystal is given by

$$S_{FE} = S_{para} + \Delta S_L + \Delta S_W, \quad (22)$$

where S_{para} is the compliance of the high symmetry phase, ΔS_L is the change in compliance due to strain/order parameter coupling, and ΔS_W is the change in compliance due to the presence of domain walls. The behavior of ΔS_W has been investigated in detail from both experimental and theoretical points of view in a series of recent papers (Schranz et al. 1999; Kityk et al. 2000a, 2000b; Harrison and Redfern 2002; Harrison et al. 2003, 2004a, 2004b, 2004c). A few relevant results are summarized here.

Following Schranz et al (1999) and Kityk et al. (2000a, 2000b), an external stress, σ, applied to a twin wall is expected to induce a strain, ε, which depends on some effective spring constant for the wall, k_W, according to Hooke's law,

$$\sigma = k_W \varepsilon. \quad (23)$$

The compliance of the wall is $1/k_W$ and the strain generated depends on the volume, ΔV_D, of material transformed from one domain to the other by displacement of a wall multiplied by the change in strain due to this transformation. The change in macroscopic strain is linearly dependent on the spontaneous strain, e_{sp}. The change in compliance is then given by

$$\Delta S_W \propto \frac{1}{k_W} \Delta V_D e_{sp}. \quad (24)$$

For an improper ferroelastic material the spontaneous strain varies as $e_{sp} \propto Q^2$. Thus if $\Delta V_D/k_W$ is constant, ΔS_W scales with Q^2 (Schranz et al. 1999; Kityk et al. 2000a, 2000b). Displacement of twin walls, which is determined by some small effective spring constant, can therefore produce a large change in the compli-

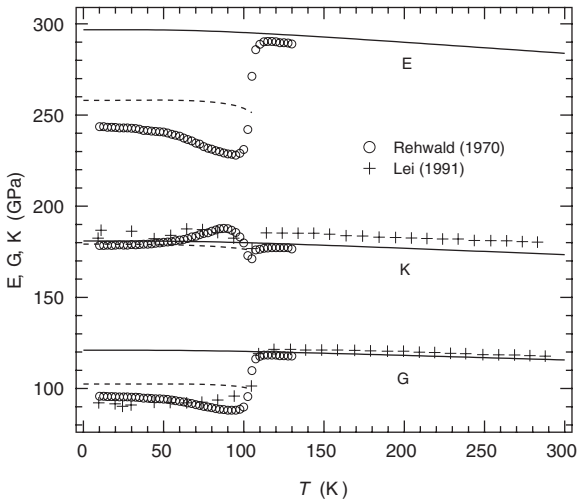

FIGURE 9. Bulk, shear, and isotropic Young's moduli for polycrystalline $SrTiO_3$, as calculated from single-crystal elastic constants. Solid lines (cubic) and broken lines (tetragonal) are calculated variations from Carpenter (2007). Pseudocubic experimental data (i.e., from twinned crystals) of Rehwald (1970) were used to calculate K, G (average of Voigt/Reuss limits) and E. Experimental values of the bulk modulus are consistent with calculated values for tetragonal $SrTiO_3$, but values for the shear modulus are smaller than values calculated assuming that the only softening is due to strain/order parameter coupling (broken line). This difference is carried through to E. [Note that there is clearly a small shift between the data of Lei (1991) and the fits to data for cubic $SrTiO_3$ given in Carpenter (2007)].

ance of the crystal, giving rise to the superelasticity of twinned ferroelastic crystals.

There are several possible mechanisms by which a twin wall can move. If it is displaced freely as a plane or is consumed/created by the retraction/advance of the tips of needle domains, $\Delta V_D/k_W$ itself can vary linearly with $1/e_{sp}$ (Harrison et al. 2004b). In this case, the change in compliance is independent of the spontaneous strain and, hence, of temperature. At the other limiting extreme, the twin domain walls may be immobilized by the pinning effects of defects located on the twin plane or at the tips of needle domains. Clearly $\Delta S_W = 0$ in this case. Pinning is a temperature-dependent process, determined by the activation energy for diffusion of the relevant defects. At high temperatures, the walls are mobile, but they become effectively frozen by the pinning process at low temperatures. A high-temperature superelastic regime (ΔS_W large and independent of T) is thus expected to be separated from a low temperature regime by a temperature interval in which "domain wall freezing" occurs (Harrison and Redfern 2002).

Two alternative situations might arise between the extremes of free wall displacements and pinned immobility. If a twin wall is pinned by defects that are located sporadically across it, some bowing might occur between the fixed points when the wall is subjected to an external stress. In this case, Equation 24 again applies. Alternatively, the twin wall movements can become blocked at high strains when walls start to interfere with each other. This is the "saturation" regime (Harrison and Redfern 2002) and the limiting strain scales linearly with e_{sp}, giving the limiting values of ΔS_W a linear dependence on Q^2. In the saturation regime bowing could still occur, however, so that there might still be some contribution of twin wall movements to the total strain.

Analysis of experimental data for $SrTiO_3$

In Dynamical Mechanical Analysis (DMA) experiments, the Young's modulus of a sample is measured at frequencies of ~1–350 Hz. Schranz et al. (1999) and Kityk et al. (2000a, 2000b) measured Young's modulus for single crystals of $SrTiO_3$ cut in different orientations at frequencies of 10, 11, and 45 Hz. Harrison et al. (2003) made similar measurements on polycrystalline samples of CST at 1 Hz. In a DMA experiment, the real part of the complex dynamical Young's modulus for, say, the [100] direction, $Y^{Re}_{[100]}$, differs from the static Young's modulus, $Y_{[100]}$, (i.e., as would be measured in a static loading experiment) by an amount that depends on any dispersion associated with the frequency at which the measurement is made and on the phase angle, δ, between the applied stress and the resultant strain (Nowick and Berry 1972). $Y^{Re}_{[100]}$is related to the absolute dynamical modulus, $Y^{abs}_{[100]}$, according to

$$Y^{Re}_{[100]} = Y^{abs}_{[100]}\cos\delta. \quad (25)$$

The phase angle is usually expressed as tanδ and the difference between $Y^{Re}_{[100]}$ and $Y^{abs}_{[100]}$ is less than 0.5% for tanδ < 0.1. All the values of tanδ given by Kityk et al. (2000a, 2000b) and Harrison et al. (2003) are less than ~0.08 so their values of $Y^{Re}_{[100]}$ have been taken to represent $Y^{abs}_{[100]}$ directly. It is further assumed here that dispersion for untwinned crystals is small, so that the absolute dynamic moduli, static moduli and moduli from ultrasonic data can be treated as being equivalent when calculating excess properties due to the presence of transformation twins.

The Young's modulus for compression or extension in the [100] direction of a cubic crystal is given by (from Nye 1985)

$$Y_{[100]} = \frac{1}{s_{11}} = \frac{\left(C_{11}-C_{12}\right)\left(C_{11}+2C_{12}\right)}{C_{11}+C_{12}}. \quad (26)$$

For a twinned tetragonal crystal with equal proportions of possible twin domain orientations

$$Y_{[100]} = \frac{1}{\frac{1}{2}\left(2s_{11}+s_{33}\right)} = \frac{3\left(C_{11}-C_{12}\right)\left[C_{33}\left(C_{11}+C_{12}\right)-2C_{13}^2\right]}{2C_{11}C_{33}-2C_{13}^2+C_{11}^2+C_{12}^2}. \quad (27)$$

For compression along the [111] direction of a cubic crystal

$$Y_{[111]} = \frac{3C_{44}\left(C_{11}+2C_{12}\right)}{C_{11}+2C_{12}+C_{44}} \quad (28)$$

and, for a tetragonal crystal

$$Y_{[111]} = \left\{\frac{1}{9}\left[\frac{2C_{33}+C_{11}+C_{12}-4C_{13}}{C_{33}\left(C_{11}+C_{12}\right)-2C_{13}^2}+\frac{2}{C_{44}}+\frac{1}{C_{66}}\right]\right\}^{-1}. \quad (29)$$

[111] is a common direction for all transformation twins created during a transformation from *m*3*m* to 4/*mmm* symmetry. For a polycrystalline sample with an isotropic distribution of grain orientations, the Young's modulus, E, is given by Equation 19 above.

The real part of the compliance, S^{Re}, for a given direction is related to the real part of the Young's modulus in DMA experiments by (from Nowick and Berry 1972)

$$S^{Re} = \frac{1}{Y^{Re}\left(1+\tan^2\delta\right)}. \quad (30)$$

For $\tan\delta < 0.1$, the error introduced by assuming $S^{Re} \approx 1/Y^{Re}$ is less than 1%, and this approximation has therefore been used when determining experimental values of S^{Re} from the data for Y^{Re} given by Kityk et al. (2000a, 2000b) and Harrison et al. (2003).

Figure 10 shows experimental values, extracted from Kityk et al. (2000b), for the compliances of single crystals measured for [100] and [111] directions using parallel plate stress (PPS) and three-point bending (TPB) methods of DMA. The original data of Kityk et al. were given relative to the values at 130 K. These have been converted to an absolute scale using values of $Y_{[100]}$ and $Y_{[111]}$ calculated for cubic $SrTiO_3$ at 130 K using the fits to C_{11}, C_{12}, and C_{44} for cubic crystals given in Carpenter (2007). Compliances equivalent to $1/Y_{[100]}$ and $1/Y_{[111]}$ for tetragonal $SrTiO_3$ have been calculated directly from the calculated values of the individual elastic constants and these are also shown in Figure 10. As found by Schranz et al. (1999) and Kityk et al. (2000a, 2000b), Equation 22 provides a good description of the experimental data for [111] TPB and [100] PPS. In this case the fits shown in Figures 10a and 10b have $1/Y_{[100]} = S_{FE} = (S_{para} + \Delta S_L) + 0.0051\, q_4^2$. Kityk et al. (2000a, 2000b) concluded that essentially the same behavior is obtained for all the other orientations that they examined by both PPS and TPB methods. Such conformance with the expected behavior is not observed for [111] PPS data, however (Fig. 10c). In this orientation, the twin walls do not experience resolved stresses that would cause them to displace (Kityk et al. 2000b), and the observed compliance is in fact smaller than the calculated compliance for an untwinned tetragonal crystal. If the twin walls in this orientation have, to a first approximation, the compliance of the para phase, they would act as a network of stiff braces through the crystal, and could shield the untwinned regions from externally applied shearing. The small change in compliance actually observed scales with q_4^2 (Fig. 10c).

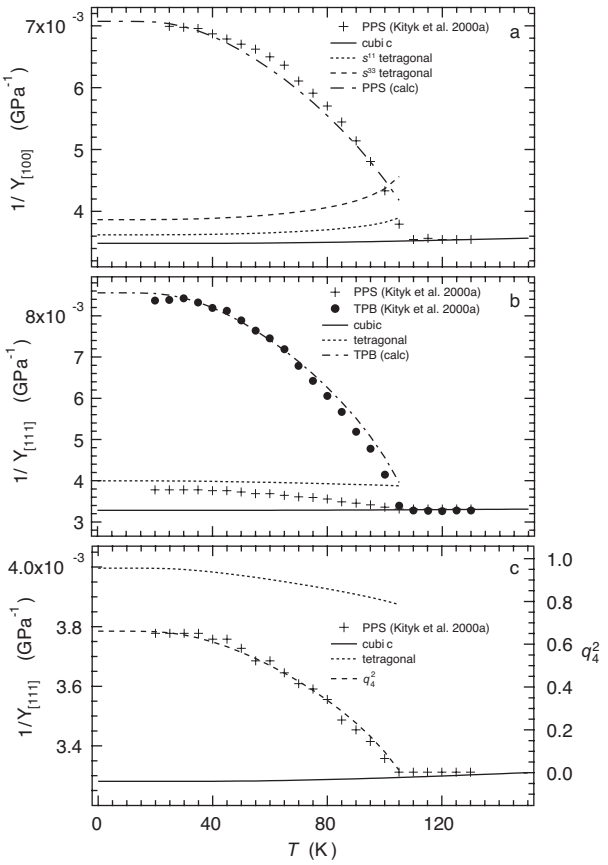

FIGURE 10. Calculated and observed compliances for (**a**) [100] and (**b**) [111] orientations of single-crystal $SrTiO_3$. The "observed" values were converted from values of the dynamical Young's modulus for PPS measurements extracted at 5 K intervals from Figures 9 and 11 of Kityk et al. (2000b). The curves for cubic $SrTiO_3$ are the calculated variations of the equivalent compliances (Eqs. 26 and 28) with values of C_{11}, C_{12}, C_{44} taken from fits to ultrasonic data (Carpenter 2007). $1/Y$ for the twinned tetragonal crystals ($= S_{para} + \Delta S_L$) was calculated using Equations 27 and 29, with values of C_{ik} for tetragonal $SrTiO_3$ from Carpenter (2007). Calculated variations (labeled "calc") are fits of Equation 22. (**c**) For PPS measurements in the [111] direction the twin walls are not expected to move, but a small change in compliance proportional to q_4^2 is observed. In this orientation, the crystal appears to be stiffer than an untwinned tetragonal crystal is predicted to be.

Analysis of experimental data for CST

Figure 11 shows the variation with temperature of the isotropic Young's modulus and related isotropic compliance for polycrystalline samples of CST70. The raw data were given by Harrison et al. (2003) as the real part of the dynamic Young's modulus, relative to the value at 769 K. These have been converted here to an absolute scale by assuming that the single-crystal elastic constants of cubic $SrTiO_3$, summarized in Carpenter (2007), provide a good estimate of the elastic properties of cubic CST at the Sr-rich end of the solid solution. Fits to the single crystal data for C_{11}, C_{12}, and C_{44} in Carpenter (2007) were used to calculate Young's modulus as a function of temperature, and a linear fit to the results for 245–300 K gave $E = 302.18 - 0.0611T$. This was extrapolated to 769 K to determine the conversion factor. It was further assumed that the real part of the dynamic Young's modulus, E^{Re}, is an adequate representation of the absolute dynamic Young's modulus and that the equivalent compliance is given by $1/E^{Re}$ ($\tan\delta < 0.08$). The experimental data cover a temperature interval of substantial superelastic softening and a lower temperature interval over which domain wall freezing occurs (Harrison et al. 2003). The samples of Harrison et al. (2003) must have had ~5% porosity, however, based on preparation of similar ceramic pellets by essentially the same method (Carpenter, unpublished data). As long as this porosity affects the elastic behavior of cubic and tetragonal samples to the same extent, the rescaling of relative values of Harrison et al. (2003) to an absolute scale for dense polycrystalline CST should still reveal the effects of the change of symmetry.

Also shown in Figure 11 are calculated variations of the isotropic Young's modulus and compliance of cubic and tetragonal samples, based on the tricritical solid-solution model presented

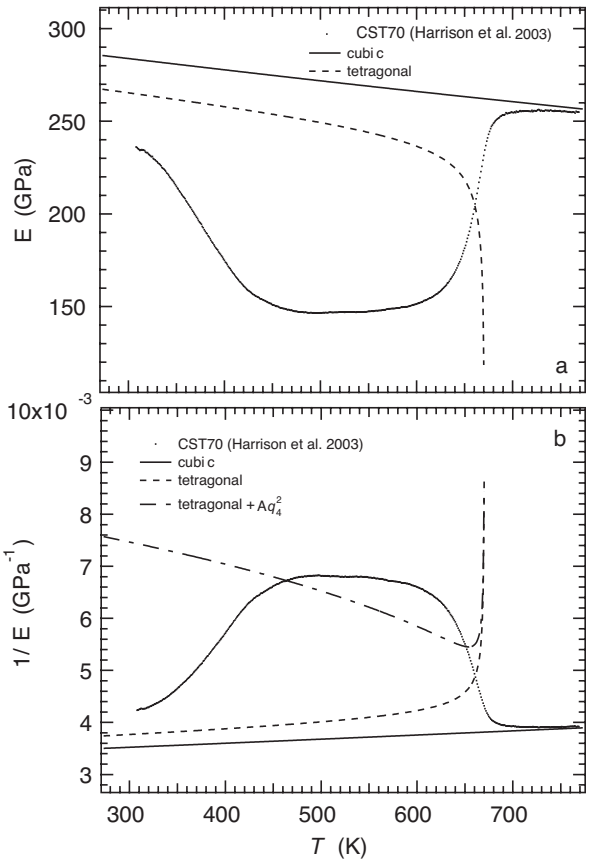

FIGURE 11. Calculated and observed variations of Young's modulus for a polycrystalline sample of CST70. *E* for cubic samples is represented by the Young's modulus of $SrTiO_3$, as calculated from fits to C_{11}, C_{12}, C_{44} (Fig. 3 of Carpenter 2007) extrapolated to high temperature. *E* for tetragonal samples was calculated by subtracting from the cubic values the softening effects of strain/order parameter coupling, as calculated for a tricritical transition ($b_2^* + b'^*_2 = 0$) with $T_c = 671$ K, $\lambda_4 = -0.131$ GPa and all other parameters listed in Table 6 of Carpenter (2007). Calculated values become relatively uncertain as $T \rightarrow T_c$; the highest temperature value shown is for 670 K. Experimental values of Harrison et al. (2003) were scaled to the value for *E* of cubic $SrTiO_3$ at 769 K. (**a**) Young's modulus. Some softening occurs ahead of the transition point, as found for single crystals (Carpenter 2007). Superelastic softening in the stability field of tetragonal crystals is almost independent of temperature before domain wall freezing effects set in below ~400 K (Harrison et al. 2003). Below the freezing interval, the observed values of *E* remain significantly smaller than the values calculated for softening due to strain/order parameter coupling alone using a simple Landau model. (**b**) Compliances, calculated from the data in **a**. Equation 22, which describes the influence of twin walls as contributing an excess compliance proportional to q_4^2, does not provide a good representation of the observed softening. The dot-dash line representing this model is shown for A = 0.0015.

above. To facilitate comparisons between observed and experimental variations, the value of $T_c = 671$ K given by Harrison et al. (2003) was used to calculate the variation of q_4 at this composition rather than $T_c = 640$ K from the fit shown in Figure 1. In principle, differences between calculated values of Young's modulus and the experimental values from Harrison et al. (2003) should be due to the influence of twin wall motion under external stress. Calculated values are shown only for $(T_c - T) \geq 1$ K because they become increasingly sensitive to the choice of parameters used in the calculations and, therefore, increasingly unreliable in the close vicinity of T_c. However Equation 22 is applied, the pattern of elastic softening is quantitatively quite different from the observed pattern. For example, the dot-dash line in Figure 11b shows $1/E$ for tetragonal crystals plus $0.0015\ q_4^2$. Even below the wall freezing interval the observed values of *E* remain smaller than the values calculated for a cubic crystal plus the effects of strain/order parameter coupling (Fig. 11a).

Equivalent calculations of *E* for each of the other CST samples described by Harrison et al. (2003) have not been undertaken but the same differences between observed and calculated values would certainly be evident for these as well. Each of the data sets in Figure 5a and data for CST60 and CST55 in Figure 7 of Harrison et al. (2003) have, however, been converted from a relative scale to an absolute scale in the same way as for CST70 to estimate values of *E* at room temperature. For CST55 this conversion is less certain because there are few data for the cubic structure. Values of *E* at ~308 K for CST68 and ~293 K for CST55, CST60, obtained in this way have been added to Figure 6. Several of the samples that are expected to be tetragonal at room temperature appear to be softer than predicted. Thus, there appears to be some degree of additional softening in polycrystalline samples, even below the freezing temperature of the domain walls. Both CST60 and CST55 are expected to be orthorhombic at room temperature but the former is close to the boundary between tetragonal and orthorhombic stability fields. CST60 has a Young's modulus that is comparable with that of tetragonal samples but CST55 is significantly stiffer. The behavior of CST85 is not understood (see Harrison et al. 2003).

DISCUSSION

To the extent that there are experimental data at different compositions across the CST system, the simple models presented here provide a surprisingly robust description of the $Pm\bar{3}m \leftrightarrow I4/mcm$ transition for the entire solid solution. Of the parameters determined for $SrTiO_3$, only two (T_{c2x} and λ_4) have been allowed to vary. This is not a unique solution as, for example, the coefficients b_2 and b'_2 could have been adjusted with λ_4 held constant, to produce tricritical behavior. In the approach adopted here, it has effectively been assumed that the incorporation of Ca into $SrTiO_3$ has a substantial effect in renormalizing λ_4 at the Sr-rich end of the solid solution. Two other distinctive characteristics of the behavior of Sr-rich CST samples are also notable. Firstly, the cubic ↔ tetragonal transition temperature varies linearly with composition between CST0 and ~CST90 (Fig. 1). There is then a distinct break in slope for ~CST90–CST100. If a progressive change in slope was simply due to saturation effects as $T_{c2} \rightarrow 0$ K, Equation 13 with $\Theta_s = 60.8$ K (from saturation in $SrTiO_3$) should have provided a better representation of the actual variation. Secondly, the additional transformation observed below ~35 K, which has been the subject of many studies (including Bednorz and Müller 1984; Bianchi et al. 1994, 1995; Dec et al. 1995; Kleemann et al. 1995, 1997; Guzhva et al. 1997), is also restricted to the composition range ~CST90 – CST100 (Fig. 1).

Replacing one cation by another with different size is, in

general, expected to give rise to local strain heterogeneities in solid solutions (Salje et al. 1991; Carpenter 1992, 2002; Hayward and Salje 1996; Redfern and Schofield 1996; Carpenter et al. 1999). Changes in such local heterogeneities with composition will then modify the extent to which a crystal is able to relax over a macroscopic length scale. In other words, the local strain behavior will result in changes to the magnitude of strain/order parameter coupling coefficients at a phase transition. From the apparently different character of the cubic-tetragonal transition at Sr-rich compositions, in comparison with the rest of the solid solution, it appears that replacing Sr by Ca induces some local strain behavior that does not extend further across the solid solution. Perhaps both λ_2 and λ_4 should increase in value; $|\lambda_2| > 0.046$ would produce a better description of the volume strains shown in Figure 3. For the transition to remain tricritical across the solid solution without adjusting the values of b_2 and b'_2, $|\lambda_4| < 0.131$ is then required, but this would also produce an improved description of the temperature and composition dependence of e_t (Fig. 3).

The evolution of the volume strain, e_a, remains only poorly characterized owing to the experimental uncertainties inherent in extrapolating the reference lattice parameter, a_o, into the stability field of the tetragonal phase. The unusual kink in transition temperature for $SrTiO_3$ as a function of pressure (Fig. 4a of Carpenter 2007, with data taken from Okai and Yoshimoto 1975) is an indirect hint that the coupling coefficient, λ_2, is not constant as a function of pressure and/or temperature, however. If the effect of increasing pressure was to suppress or modify local strain heterogeneities, the strength of coupling between q_4 and e_a might increase, providing a mechanism for some pressure dependence of λ_2.

Hidden but potentially influential parameters in the solid solution model presented here are the coupling coefficient λ_5 and the susceptibility, χ_6. λ_5 describes coupling between the order parameter and the strain e_4, and contributes to softening of C_{44}. As $e_4 \equiv 0$ in the tetragonal structure, there are no strain data against which to test directly the assumption that λ_5 remains constant across the solid solution. C_{44} is also sensitive to the value of the coupling coefficient λ_4 through the equation for χ_6^{-1} (Table 1). A test of models of elastic behavior in this system would clearly be to measure the variation of C_{44} in single crystals of CST perovskite. For the present it should be noted that only ~2/5 of changes in C_{44} contribute to changes in the shear modulus. This is evident from equations for C_{44} and the Voigt shear modulus given in Table 2 of Carpenter (2007). Thus any additional softening in G_V of, say, 10 GPa would be accompanied by an additional softening of ~25 GPa in C_{44} if changes in λ_5 or χ_6^{-1} were the cause.

The solid-solution model has permitted some reanalysis of the excess elastic softening associated with the two known styles of anelastic softening in tetragonal CST. In $SrTiO_3$ the additional softening is consistent with the model of Schranz et al. (1999) and Kityk et al. (2000a, 2000b), i.e., Equation 22 describes the observed elastic behavior quantitatively for selected orientations, with no evidence of any wall pinning/freezing. The same model does not describe the temperature-independent softening in polycrystalline CST found by Harrison et al. (2003). On the other hand, it leads to the suggestion that even below the temperature interval of domain wall freezing, the data of Harrison et al. (2003) perhaps imply a degree of softening that is greater than could be due to strain/order parameter coupling alone. One simple interpretation of these conflicting results is that the temperature-independent softening is due to the motion of twin needle tips and twin wall rotations, while the low-temperature anelastic contributions are due to twin wall motions alone. Harrison et al. (2004a, 2004b, 2004c) have already reported a change in the relative importance of these two mechanisms as a function of temperature in $LaAlO_3$ and lead orthophosphate. The susceptibility of needle tips and twin walls to pinning is presumably somewhat different. Alternatively, the low-temperature anelastic effects are due to bowing of the walls between pinning points.

As with superelastic softening at high temperatures (Harrison et al. 2003), the effect of transforming from tetragonal to orthorhombic symmetry is to cut off, more or less abruptly, the softening displayed by CST at room temperature (Fig. 6 and see Carpenter et al. 2007). In this context, it is notable that the tetragonal strain in CST crystals with *Pnma* symmetry is close to zero (Carpenter et al. 2001). This occurs because the strain depends on the separate order parameter components associated with M point and R point tilting (q_2 and q_4, respectively) according to (from Carpenter et al. 2001)

$$e_{tx} = -\frac{2\left(\lambda_3 q_2^2 - \lambda_4 q_4^2\right)}{\frac{1}{2}\left(C_{11}^o - C_{12}^o\right)}. \quad (31)$$

Here, λ_3 and λ_4 are the coupling coefficients for q_2 and q_4 that give rise to a tetragonal strain, e_{tx}, oriented along the X-axis of the reference system. Each tilt couples in the same way with the strain (λ_3, λ_4 have the same sign), but the net effect is $e_{tx} \approx 0$. In other words, even if the application of a shear stress to a domain wall could cause some displacement, there is effectively no change in the macrosopic strain. Domain wall motion as a mechanism for superelastic softening would then be negated.

Finally, no attempt has yet been made to explain the stability of the *Pnma* structure in this system. Half the coefficients of the master equation (Eq. 1 of Carpenter 2007) are now known with a reasonable degree of confidence, however, and a full thermodynamic description of the *I*4/*mcm* ↔ *Pnma* transition has been brought a stage closer. For present purposes, it is sufficient to note that the trend from second order character toward tricritical for the R point transition is exactly the direction of change required to cause a *Pnma* structure to become more stable than a *Cmcm* structure below the critical temperature of both the M and R point instabilities (Carpenter 2007). Thus the strength of strain/order parameter coupling may be a key factor in determining the relative stability of these structures in CST perovskites.

ACKNOWLEDGEMENTS

This work was funded by a grant from the Natural Environment Research Council (NER/A/S/2000/01055), which is gratefully acknowledged. F. Seifert is thanked for providing original heat capacity data from the work of Qin et al. (2000), and C.J. Howard for data relating to CST70 from the work of Howard et al. (2005).

REFERENCES CITED

Ali, R. and Yashima, M. (2005) Space group and crystal structure of the perovskite $CaTiO_3$ from 296 to 1720 K. Journal of Solid State Chemistry, 178, 2867–2872.

Ball, C.J., Begg, B.D., Cookson, D.J., Thorogood, G.J., and Vance, E.R. (1998) Structures in the system $CaTiO_3/SrTiO_3$. Journal of Solid State Chemistry, 139, 238–247.

Beattie, A.G. and Samara, G.A. (1971) Pressure dependence of the elastic constants of $SrTiO_3$. Journal of Applied Physics, 42, 2376–2381.

Bednorz, J.G. and Müller, K.A. (1984) $Sr_{1-x}Ca_xTiO_3$: An XY quantum ferroelectric with transition to randomness. Physical Review Letters, 52, 2289–2292.

Bianchi, U. (1996) Glasartiges Verhalten, Ferroelektrizität und photoinduzierte Effekte in Strontium-Kalzium-Titanit ($Sr_{1-x}Ca_xTiO_3$, $0 \le x \le 0.12$). Ph.D. thesis, Gerhard-Marcator University, Duisburg.

Bianchi, U., Kleemann, W., and Bednorz, J.G. (1994) Raman scattering of ferroelectric $Sr_{1-x}Ca_xTiO_3$, x = 0.007. Journal of Physics: Condensed Matter, 6, 1229–1238.

Bianchi, U., Dec, J., Kleemann, W., and Bednorz, J.G. (1995) Cluster and domain-state dynamics of ferroelectric $Sr_{1-x}Ca_xTiO_3$ (x = 0.007). Physical Review B, 51, 8737–8746.

Binder, A. and Knorr, K. (2001) Shear elasticity and ferroelastic hysteresis of the low-temperature phase of $SrTiO_3$. Physical Review B, 63, 094106.

Bonello, B., Fischer, M., and Zarembowitch, A. (1989a) Acoustical measurements in solids under very high pressure. Ultrasonics, 27, 343–348.

Bonello, B., Fischer, M., and Polian, A. (1989b) Phase transition and sound velocity measurements in very small solid samples under high pressure by Brillouin scattering. Journal of the Acoustical Society of America, 86, 2257–2260.

Brugger, K. (1965) Pure modes for elastic waves in crystals. Journal of Applied Physics, 36, 759–768.

Carpenter, M.A. (1992) Thermodynamics of phase transitions in minerals: a macroscopic approach. In G.D. Price and N.L. Ross, Eds., The stability of minerals, p. 172–215. Chapman and Hall, London.

——— (2002) Microscopic strain, macroscopic strain and the thermodynamics of phase transitions in minerals. European Mineralogical Union Notes in Mineralogy, 4, 311–346.

——— (2007) Elastic anomalies accompanying phase transitions in (Ca,Sr)TiO_3 perovskites: Part I. Landau theory and a calibration for $SrTiO_3$. American Mineralogist, 92, 309–327.

Carpenter, M.A. and Salje, E.K.H. (1998) Elastic anomalies in minerals due to structural phase transitions. European Journal of Mineralogy, 10, 693–812.

Carpenter, M.A., Boffa Ballaran, T., and Atkinson, A.J. (1999) Microscopic strain, local structural heterogeneity and the energetics of silicate solid solutions. Phase Transitions 69, 95–109.

Carpenter, M.A., Becerro, A.I., and Seifert, F. (2001) Strain analysis of phase transitions in (Ca,Sr)TiO_3 perovskites. American Mineralogist, 86, 348–363.

Carpenter, M.A., Li, B., and Liebermann, R.C. (2007) Elastic anomalies accompanying phase transitions in (Ca,Sr)TiO_3 perovskites: Part III. Experimental investigation of polycrystalline samples. American Mineralogist, 92, 344–355.

Cowley, R.A. (1996) The phase transition in strontium titanate. Philosophical Transactions of the Royal Society of London A, 354, 2799–2814.

Dec, J., Kleemann, W., Bianchi, U., and Bednorz, J.G. (1995) Glass-like interacting off-centre Ca^{++} dipoles as probes of the "coherent quantum state" in $SrTiO_3$. Europhysics Letters, 29, 31–36.

Fischer, M., Bonnello, B., Polian, A., and Léger, J.-M. (1989) Elasticity of $SrTiO_3$ perovskite under high pressure. In A. Navrotsky and D.J. Weidner, Eds., Perovskite: a structure of great interest to Geophysics and Materials Science. Geophysical Monograph, 45, 125–130.

Fossheim, K. and Berre, B. (1972) Ultrasonic propagation, stress effects, and interaction parameters at the displacive transition in $SrTiO_3$. Physical Review B, 5, 3292–3308.

Gallardo, M.C., Becerro, A.I., Romero, F.J., del Cerro, J., Seifert, F., and Redfern, S.A.T. (2003) Cubic-tetragonal phase transition in $Ca_{0.04}Sr_{0.96}TiO_3$: a combined specific heat and neutron diffraction study. Journal of Physics: Condensed Matter, 15, 91–100.

Gillet, P., Guyot, F., Price, G.D., Tournerie, B., and Le Cleach, A. (1993) Phase changes and thermodynamic properties of $CaTiO_3$. Spectroscopic data, vibrational modelling and some insights on the properties of $MgSiO_3$ perovskite. Physics and Chemistry of Minerals, 20, 159–170.

Grzechnik, A., Wolf, G.H., and McMillan, P.F. (1997) Raman scattering study of $SrTiO_3$ at high pressure. Journal of Raman Spectroscopy, 28, 885–889.

Guyot, F., Richet, P., Courtial, Ph., and Gillet, Ph. (1993) High-temperature heat capacity and phase transitions of $CaTiO_3$ perovskite. Physics and Chemistry of Minerals, 20, 141–146.

Guzhva, M.E., Markovin, P.A., and Kleemann, W. (1997) Spontaneous photorefractive effect in $Sr_{1-x}Ca_xTiO_3$ (x = 0.014). Physics of the Solid State, 39, 625–627.

Harrison, R.J. and Redfern, S.A.T. (2002) The influence of transformation twins on the seismic-frequency elastic and anelastic properties of perovskite: dynamical mechanical analysis of single crystal $LaAlO_3$. Physics of the Earth and Planetary Interiors, 134, 253–272.

Harrison, R.J., Redfern, S.A.T., and Street, J. (2003) The effect of transformation twins on the seismic-frequency mechanical properties of polycrystalline $Ca_{1-x}Sr_xTiO_3$ perovskite. American Mineralogist, 88, 574–582.

Harrison, R.J., Redfern, S.A.T., and Salje, E.K.H. (2004a) Dynamical excitation and anelastic relaxation of ferroelastic domain walls in $LaAlO_3$. Physical Review B, 69, 144101.

Harrison, R.J., Redfern, S.A.T., and Bismayer, U. (2004b) Seismic-frequency attenuation at first-order phase transitions: dynamical mechanical analysis of pure and Ca-doped lead orthophosphate. Mineralogical Magazine, 68, 839–852.

Harrison, R.J., Redfern, S.A.T., Buckley, A., and Salje, E.K.H. (2004c) Application of real-time, stroboscopic X-ray diffraction with dynamical mechanical analysis to characterize the motion of ferroelastic domain walls. Journal of Applied Physics, 95, 1706–1717.

Hayward, S.A. and Salje, E.K.H. (1996) Displacive phase transition in anorthoclase: the "plateau effect" and the effect of T1-T2 ordering on the transition temperature. American Mineralogist, 81, 1332–1336.

——— (1998) Low-temperature phase diagrams: non-linearities due to quantum mechanical saturation of order parameters. Journal of Physics: Condensed Matter, 10, 1421–1430.

——— (1999) Cubic-tetragonal phase transition in $SrTiO_3$ revisited: Landau theory and transition mechanism. Phase Transitions, 68, 501–522.

Howard, C.J. and Stokes, H.T. (1998) Group-theoretical analysis of octahedral tilting in perovskites. Acta Crystallographica B, 54, 782–789.

Howard, C.J., Withers, R.L., and Kennedy, B.J. (2001) Space group and structure for the perovskite $Ca_{0.5}Sr_{0.5}TiO_3$. Journal of Solid State Chemistry, 160, 8–12.

Howard, C.J., Withers, R.L., Zhang, Z., Osaka, K., Kato, K., and Takata, M. (2005) Space-group symmetry for the perovskite $Ca_{0.3}Sr_{0.7}TiO_3$. Journal of Physics: Condensed Matter, 17, L459–465.

Ishidate, T. and Isonuma, T. (1992) Phase transition of $SrTiO_3$ under high pressure. Ferroelectrics, 137, 45–52.

Ishidate, T., Sasaki, S., and Inoue, K. (1988) Brillouin scattering of $SrTiO_3$ under high pressure. High Pressure Research, 1, 53–65.

Kennedy, B.J., Howard, C.J., and Chakoumakos, B.C. (1999) Phase transitions in perovskite at elevated temperatures—a powder neutron diffraction study. Journal of Physics: Condensed Matter, 11, 1479–1488.

Kityk, A.V., Schranz, W., Sondergeld, P., Havlik, D., Salje, E.K.H., and Scott, J.F. (2000a) Low-frequency superelasticity and nonlinear elastic behavior of $SrTiO_3$ crystals. Physical Review B, 61, 946–956.

——— (2000b) Nonlinear elastic behaviour of $SrTiO_3$ crystals in the quantum paraelectric regime. Europhysics Letters, 50, 41–47.

Kleemann, W., Bianchi, U., Bürgel, A., Prasse, M., and Dec, J. (1995) Domain state properties of weakly doped $SrTiO_3$:Ca. Phase Transitions, 55, 57–68.

Kleemann, W., Albertini, A., Kuss, M., and Lindner, R. (1997) Optical detection of symmetry breaking on a nanoscale in $SrTiO_3$:Ca. Ferroelectrics, 203, 57–64.

Lei, M. (1991) Oxides and oxide superconductors: elastic and related properties. Ph.D. dissertation, University of Colorado, Boulder.

Lemanov, V.V. (1997) Phase transitions in $SrTiO_3$-based solid solutions. Physics of the Solid State, 39, 1468–1473.

Lemanov, V.V., Gridnev, S.A., and Ukhin, E.V. (2002) Low-frequency elastic properties, domain dynamics, and spontaneous twisting of $SrTiO_3$ near the ferroelastic phase transition. Physics of the Solid State, 44, 1156–1165.

Mishra, S.K., Ranjan, R., Pandey, D., and Kennedy, B.J. (2002) Powder neutron diffraction study of the antiferroelectric phase transition in $Sr_{0.75}Ca_{0.25}TiO_3$. Journal of Applied Physics, 91, 4447–4452.

Mishra, S.K., Ranjan, R., Pandey, D., Ranson, P., Ouillon, R., Pinan-Lucarre, J.-P., and Pruzan, P. (2005) A combined X-ray diffraction and Raman scattering study of the phase transitions in $Sr_{1-x}Ca_xTiO_3$ ($x = 0.04, 0.06, 0.12$). Journal of Solid State Chemistry, 178, 2846–2857.

Mishra, S.K., Ranjan, R., Pandey, D., and Stokes, H.T. (2006a) Resolving the controversies about the 'nearly cubic' and other phases of $Sr_{1-x}Ca_xTiO_3$ ($0 \le x \le 1$): I. Room temperature structures. Journal of Physics: Condensed Matter, 18, 1885–1898.

Mishra, S.K., Ranjan, R., Pandey, D., Ranson, P., Ouillon, R., Pinan-Lucarre, J.-P., and Pruzan, P. (2006b) Resolving the controversies about the 'nearly cubic' and other phases of $Sr_{1-x}Ca_xTiO_3$ ($0 \le x \le 1$): II. Comparison of phase transition behaviours for $x = 0.40$ and 0.43. Journal of Physics: Condensed Matter, 18, 1899–1912.

Mitsui, T. and Westphal, W.B. (1961) Dielectric and X-ray studies of $Ca_xBa_{1-x}TiO_3$ and $Ca_xSr_{1-x}TiO_3$. Physical Review, 124, 1354–1359.

Nowick, A.S. and Berry, B.S. (1972) Anelastic relaxation in crystalline solids, 677 p. Academic Press, New York.

Nye, J.F. (1985) Physical properties of crystals, 329 p. Oxford University Press, U.K.

Okai, B. and Yoshimoto, J. (1975) Pressure dependence of the structural phase transition temperature in $SrTiO_3$ and $KMnF_3$. Journal of the Physical Society of Japan, 39, 162–165.

Ouillon, R., Pinan-Lucarre, J.-P., Ranson, P., Pruzan, Ph., Mishra, S.K., Ranjan, R., and Pandey, D. (2002) A Raman scattering study of the phase transitions in $SrTiO_3$ and in the mixed system $(Sr_{1-x}Ca_x)TiO_3$ at ambient pressure from $T = 300$ K down to 8 K. Journal of Physics: Condensed Matter, 14, 2079–2092.

Qin, S., Becerro, A.I., Seifert, F., Gottsmann, J., and Jiang, J. (2000) Phase transitions in $Ca_{1-x}Sr_xTiO_3$ perovskites: effects of composition and temperature. Journal of Materials Chemistry, 10, 1609–1615.

Qin, S., Wu, X., Seifert, F., and Becerro, A.I. (2002) Micro-Raman study of perovskites in the $CaTiO_3$–$SrTiO_3$ system. Journal of the Chemical Society,

Dalton Transactions, 2002, 3751–3755.
Ranjan, R. and Pandey, D. (1999) Novel structural features and phase transition behaviour of $(Sr_{1-x}Ca_x)TiO_3$: II. X-ray diffraction studies. Journal of Physics: Condensed Matter, 11, 2247–2258.
——— (2001a) Antiferroelectric phase transition in $(Sr_{1-x}Ca_x)TiO_3$ ($0.12 < x \leq 0.40$): I. Dielectric studies. Journal of Physics: Condensed Matter, 13, 4239–4249.
——— (2001b) Antiferroelectric phase transition in $(Sr_{1-x}Ca_x)TiO_3$: II. X-ray diffraction studies. Journal of Physics: Condensed Matter, 13, 4251–4266.
Ranjan, R., Pandey, D., Siruguri, V., Krishna, P.S.R., and Paranjpe, S.K. (1999) Novel structural features and phase transition behaviour of $(Sr_{1-x}Ca_x)TiO_3$: I. Neutron diffraction study. Journal of Physics: Condensed Matter, 11, 2233–2246.
Ranjan, R., Pandey, D., and Lalla, N.P. (2000) Novel features of $Sr_{1-x}Ca_xTiO_3$ phase diagram: evidence for competing antiferroelectric and ferroelectric interactions. Physical Review Letters, 84, 3726–3729.
Ranjan, R., Pandey, D., Schuddinck, W., Richard, O., De Meulenaere, P., Van Landuyt, J., and Van Tendeloo, G. (2001) Evolution of crystallographic phases in $(Sr_{1-x}Ca_x)TiO_3$ with composition (x). Journal of Solid State Chemistry, 162, 20–28.
Ranson, P., Ouillon, R., Pinan-Lucarre, J.-P., Pruzan, Ph., Mishra, S.K., and Ranjan, R. (2005) The various phases of the system $Sr_{1-x}Ca_xTiO_3$—a Raman scattering study. Journal of Raman Spectroscopy, 36, 898–911.
Redfern, S.A.T. (1996) High-temperature structural phase transitions in perovskite ($CaTiO_3$). Journal of Physics: Condensed Matter, 8, 8267–8275.
Redfern, S.A.T., and Schofield, P.F. (1996) Order parameter saturation (plateau effect) as a function of composition in the sanmartinite ($ZnWO_4$)–cuproscheelite ($CuWO_4$) solid solution. Phase Transitions, 59, 25–38.
Rehwald, W. (1970) Low temperature elastic moduli of strontium titanate. Solid State Communications, 8, 1483–1485.
——— (1971) Ultrasonic properties of strontium titanate at the 105 K transition. Physik der Kondensierten Materie, 14, 21–36.
Ross, N.L. and Angel, R.J. (1999) Compression of $CaTiO_3$ and $CaGeO_3$ perovskites. American Mineralogist, 84, 277–281.
Salje, E.K.H., Bismayer, U., Wruck, B., and Hensler, J. (1991) Influence of lattice imperfections on the transition temperatures of structural phase transitions: the plateau effect. Phase Transitions, 35, 61–74.
Salje, E.K.H., Gallardo, M.C., Jiménez, J., Romero, F.J., and del Cerro, J. (1998) The cubic-tetragonal phase transition in strontium titanate: excess specific heat measurements and evidence for a near-tricritical, mean field type transition mechanism. Journal of Physics: Condensed Matter, 10, 5535–5543.
Schranz, W., Sondergeld, P., Kityk, A.V., and Salje, E.K.H. (1999) Elastic properties of $SrTiO_3$ crystals at ultralow frequencies. Phase Transitions, 69, 61–76.
Slonczewski, J.C. and Thomas, H. (1970) Interaction of elastic strain with the structural transition of strontium titanate. Physical Review B, 1, 3599–3608.
Watt, J.P. and Peselnik. L. (1980) Clarification of the Hashin-Shtrikman bounds on the effective elastic moduli of polycrystals with hexagonal, trigonal, and tetragonal symmetries. Journal of Applied Physics, 51, 1525–1531.
Woodward, D.I., Wise, P.L., Lee, W.F., and Reaney, I.M. (2006) Space group symmetry of $(Ca_xSr_{1-x})TiO_3$ determined using electron diffraction. Journal of Physics: Condensed Matter, 18, 2401–2408.
Yamanaka, T., Hirai, N., and Komatsu, Y. (2002) Structure change of $Ca_{1-x}Sr_xTiO_3$ perovskite with composition and pressure. American Mineralogist, 87, 1183–1189.

MANUSCRIPT RECEIVED APRIL 27, 2006
MANUSCRIPT ACCEPTED SEPTEMBER 28, 2006
MANUSCRIPT HANDLED BY GEORGE LAGER